Portland State University
PDXScholar

Dissertations and Theses

Dissertations and Theses

5-24-1994

Magmatic Evolution and Eruptive History of the Granitic Bumping Lake Pluton, Washington: Source of the Bumping River and Cash Prairie Tuffs

John Frederick King
Portland State University

Follow this and additional works at: https://pdxscholar.library.pdx.edu/open_access_etds

 Part of the Geology Commons

Let us know how access to this document benefits you.

Recommended Citation
King, John Frederick, "Magmatic Evolution and Eruptive History of the Granitic Bumping Lake Pluton, Washington: Source of the Bumping River and Cash Prairie Tuffs" (1994). *Dissertations and Theses.* Paper 4765.
https://doi.org/10.15760/etd.6649

This Thesis is brought to you for free and open access. It has been accepted for inclusion in Dissertations and Theses by an authorized administrator of PDXScholar. Please contact us if we can make this document more accessible: pdxscholar@pdx.edu.

THESIS APPROVAL

The abstract and thesis of John Frederick King for the Master of Science in Geology were presented May 24, 1994, and accepted by the thesis committee and the department.

COMMITTEE APPROVALS:

[redacted]
Paul E. Hammond, Chair

[redacted]
Ansel G. Johnson

[redacted]
Mark T. Murphy, Senior Research Scientist
Pacific Northwest Laboratories

[redacted]
Dennis Barnum
Representative of the Office of Graduate Studies

DEPARTMENT APPROVAL:

[redacted]
Marvin H. Beeson, Chair
Department of Geology

* *

ACCEPTED FOR PORTLAND STATE UNIVERSITY BY THE LIBRARY

by [redacted] on 9 August 1994

ABSTRACT

An abstract of the thesis of John Frederick King for the Master of Science in Geology presented May 24, 1994.

Title: Magmatic Evolution and Eruptive History of the Granitic Bumping Lake Pluton, Washington: Source of the Bumping River and Cash Prairie Tuffs.

The 25 Ma Bumping Lake pluton ranges in composition from quartz diorite to granite with the granitic facies comprising approximately 90% of the pluton's surface area. The granite may be classified as calcalkaline, peraluminous and I-type with some S-type characteristics. A late-stage, mafic-poor facies fills cooling related extensional fractures. The pluton was passively emplaced into the Ohanapecosh Formation at a shallow level in the crust. Contact relationships vary from sharp where the contact is vertical to gradational at the roof of the pluton. Where gradational, stoped xenoliths from the roof of the pluton increase in size, angularity and retain more of their primary textures as the contact is approached. Spacial trends in major and trace elements support the interpretation that xenoliths were stoped and assimilated into the melt. The predicted Rayleigh number for the pluton when molten is 10^{7} and the predicted Reynolds number is approximately 10^{-9}. Based on these values, the magma of the pluton probably did not convect, and if it did, convection was weak and not a significant process.

Based on variations in Eu/Eu* and Sr values, plagioclase fractionation was an important process in the petrogenesis of the pluton. Additionally, fractionation of accessory minerals rich in light rare-earth elements (LREE) resulted in successive depletion of LREE with progressive differentiation. Two separate regions of the pluton are highly differentiated as indicated by high SiO_2 values, high Rb/Zr ratios, and low Zr and TiO_2 values.

Mapping by the author indicates that the pluton projects beneath the Mount Aix caldera. Dates of three tuffs derived from the caldera are equivalent to the pluton, and two of these tuffs are chemically indistinguishable from the granite facies of the pluton. This implies that the Bumping Lake pluton represents the chilled remains of the magma chamber that fed the Mount Aix caldera.

MAGMATIC EVOLUTION AND ERUPTIVE HISTORY OF THE GRANITIC BUMPING LAKE PLUTON, WASHINGTON: SOURCE OF THE BUMPING RIVER AND CASH PRAIRIE TUFFS

by

JOHN FREDERICK KING

A thesis submitted in partial fulfillment of the
requirements for the degree of

MASTER OF SCIENCE
in
GEOLOGY

Portland State University
1994

ACKNOWLEDGMENTS

First and foremost, my wife, Kirsti, deserves my deepest gratitude for enduring my absence: whether physically while I was working in the field or the lab, or mentally while I was analyzing data and writing this thesis. She also provided excellent help with formatting the text, tables, and figures. I am also thankful of my parents' support and their patience when I would get excited and tell them more than they probably wanted to hear about my findings. My graduate advisor, Paul Hammond, provided excellent guidance through the entire project as well as many appreciated recommendations for grants, and thoughtful criticisms and reviews of publications leading up to and including this thesis. Peter Hooper and his co-workers at Washington State University's GeoAnalytical Laboratory made it financially possible for me to analyze my samples and provided excellent service. Kay Kendall and Eric Lepire were kind enough to allow me to work on my thesis when things were slow at work and I had a long way to go. Thanks also to my office mates Judy Passman, Keith Brunstad, and Michelle Barnes, who lended a critical ear to my ideas and interpretations. I also gratefully acknowledge grants from the Geological Society of America and Sigma Xi.

TABLE OF CONTENTS

LIST OF TABLES

LIST OF FIGURES

INTRODUCTION

Attempts to model high-silica magma chambers have traditionally relied on stratigraphic studies of material erupted from the chambers rather than studies of the chambers themselves (e.g., Williams, 1942; Katsui, 1963; Smith, 1966; Hildreth, 1979; Fridrich and Mahood, 1987; Bacon and Druitt, 1988; Whitney, 1988). These studies are meaningful, but are limited in that they can only provide information about the chamber at a few instants throughout the life of the chamber. Additional or at least more conclusive information might be retrieved from the system if the magma chamber *and* its eruptive products are studied.

It is uncommon for both a crystallized magma chamber and its eruptive products to be exposed in sufficient detail to permit an investigation relating the two. A magma chamber is usually exposed only after the pile of volcanic material above is eroded away, which is self-defeating because an associated volcanic pile is the best evidence that a pluton was also a magma chamber. Without an association of volcanic material, it is unlikely that a crystallized magma chamber could be distinguished from an intrusion with no associated vent.

Mapping by Abbott (1953), Campbell (1987), and the author (Hammond and others, 1993) shows that the Bumping Lake pluton is a large granitic body exposed within 400 m of the Mount Aix caldera. One zircon fission-track date of the pluton of 24.7±0.6 Ma is reported by Clayton (1983). K-Ar and zircon fission-track dates of quartz-bearing

tuffs from the caldera fill complex range from 27.6±1.4 Ma (Schreiber, 1981) to 26.3±1.3 Ma (Vance and others, 1987). The above relationships indicate that the pluton may be the crystallized remains of the magma chamber that once fed the Mount Aix caldera.

OBJECTIVES

The primary purpose of this research is to substantiate the existence of a cogenetic relationship between the Bumping Lake pluton and the Mount Aix caldera. To this end, physical features, petrography and chemistry of the pluton are described in detail and compared to the caldera and its eruptive products. Establishment of the pluton as a volcanic source allows the pluton to be viewed as a complex and dynamic system. Having this knowledge allows a more thorough understanding of the magmatic processes that an active magma chamber can be subject to.

METHODS OF STUDY

The problem of relating a plutonic body to alleged eruptive products should be attacked on multiple fronts so that one method can be used to support or deny interpretations based on another method. In this study, field relationships provide the foundation for the rest of the study. Only when the field work is complete and understood do chemical and petrographic data have meaning. For this study, all analyses were performed at Washington State University's GeoAnalytical Lab. Of 154 total samples from the pluton, 138 were analyzed by XRF (Appendix B). Representative samples of this group were analyzed by ICP-MS (Appendix C). Twelve samples were examined pet-

rographically. Additionally, 47 samples of three tuffs were analyzed by XRF, and representative samples from each tuff were also analyzed by ICP-MS. Thin sections of each tuff were examined and compared to the thin sections of the pluton.

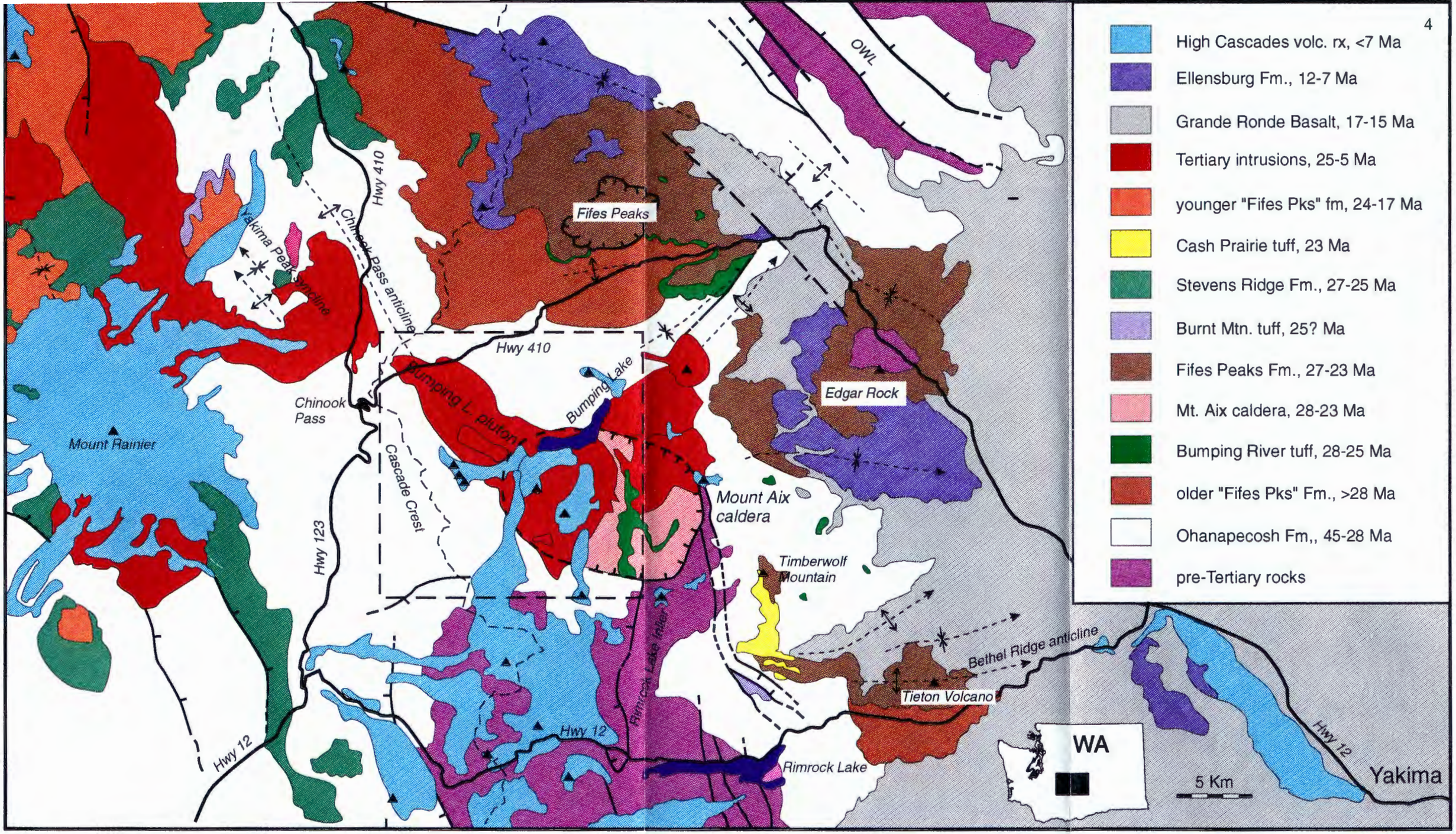

Figure 1. Geologic setting of the Bumping Lake pluton. Dashed box represents the area shown in Figure 2.

GEOLOGIC SETTING

The Cascade Range is a 1100 km long continental arc that has been active since its inception at about 42 Ma (Atwater, 1970; Duncan and Kulm, 1989). Early in the margin's history, the convergence rate was relatively rapid and steep (Riddihough, 1984). Although the convergence rate has varied throughout the life of the margin, on average, the convergence rate and the subduction angle has been decreasing (Riddihough, 1984). Over time, continued volcanism in the arc increased the local heat flow gradient, which allowed large felsic bodies to ascend to shallow levels in the continental crust. Some of these bodies vented to the surface and produced about 20 quartz-bearing tuffs that are widely scattered through the Cascade Range and vary in age from 36-18 Ma (Paul E. Hammond, pers. commun., 1994). The granitic Bumping Lake pluton and its associated vent, the Mount Aix caldera, are an example of one of these tuff-producing intrusive/volcanic systems (Figure 1).

RIMROCK LAKE INLIER

The Rimrock Lake inlier is composed of five pre-Tertiary units separated along vertical tectonic contacts or shear faults, which do not extend into younger units (Schasse, 1987; Walsh and others, 1987). The inlier is about 25 by 40 km in outcrop and to the south, reaches within two kilometers of the Bumping Lake pluton. Pre-arc sedimentary rocks sporadically overlie the inlier. The strata are thinner in the vicinity of the

pluton than to the east and west, which indicates that the inlier formed a structural high in the early Tertiary. The present structural and topographic high is just south of Rimrock Lake. From there the structural high dips gently to the north and projects beneath the Bumping Lake pluton. To the east of the pluton, it is truncated by the caldera margin fault of the Mount Aix caldera.

The upper Jurassic to lower Cretaceous Russell Ranch Formation is one of the five units within the inlier and consists primarily of metasedimentary rocks that show turbidite characteristics of the flysch facies (Schasse, 1987). The Lookout Formation is older than 157 Ma and consists chiefly of black graphitic garnet-mica schist and amphibolite, minor metatonalite, metagranodiorite, and metagabbro (Walsh and others, 1987; Schasse, 1987). Foliated metaplutonic rock of Indian Creek is late Jurassic to early Cretaceous in age and consists of two north-striking belts of predominantly tonalite, minor gabbro, diorite, amphibolite, and schist (Miller, 1989). North of Edgar Rock, Walsh and others (1987) and Schasse (1987) describe the occurrence of dark green greenstones and dikes that may be early Tertiary in age. Walsh and others (1987) and Schasse (1987) also describe a Mesozoic unit weakly associated with the Russell Ranch Formation that is chiefly cataclastic amphibolite, with minor phyllite, greenstone, schist, gneiss, metasandstone, and ultramafite.

OHANAPECOSH FORMATION

In all cases, rocks of the Oligocene Ohanapecosh Formation constitute the intrusive host. Radiometric dates on tuffs throughout the formation range from 28±2.9 to

36.4±3.6 Ma (Schasse, 1987; Vance and others, 1987). The Ohanapecosh Formation is a thick sequence of intermediate composition lithic breccias, lava flows, and lithic-lapilli tuffs, volcaniclastic siltstone, sandstone, and conglomerate (Fiske and others, 1963; Winters, 1984; Schasse, 1987; Vance and others, 1987).

Although intrusive relations range from gradational to relatively sharp, in all cases rocks of the Ohanapecosh constitute the intrusive host. Where gradational, the intrusion filled fractures in the host rock and then solidified so that fragments of the host rock can be visually pieced back together. Near the intrusive contact, textures and compositions of the xenoliths closely resemble those found in Ohanapecosh rocks. As distance from the contact increases, xenolithic textures become less varied and their size and frequency decrease. Typically this transition takes place over a distance of approximately 200 vertical meters. Based on this size, frequency, textural, and compositional evidence, these xenoliths are interpreted to be stoped country rock rather than parental melt. Light-colored reaction rims surround many xenoliths near Chinook Pass, but are absent around enclaves found on Miners Ridge. Sharp intrusive contacts are less common, but can be found on American Ridge and to the west on a ridge south of Cougar Lake. At these locations, xenoliths are absent and the distance over which the pluton grades into the host rock is typically about two meters.

A NW-SE trending anticline in the Ohanapecosh Formation probably existed prior to emplacement of the pluton since no deformation is apparent in the pluton. The anticlinal axis is parallel to the long axis of the pluton and may have influenced the location of the intrusion. Lack of faulting or structurally disturbed beds in the Ohanapecosh For-

mation surrounding the pluton suggests it was emplaced without deforming its host. The extent to which the country rock is metamorphosed is surprisingly low and is on the order of 10 to 100 meters.

Wildcat Creek Beds

Wildcat Creek beds are well-bedded, andesitic and dacitic volcaniclastic rocks (Swanson, 1978; Schreiber, 1981) that have been dated at 32.2 ±3.3 and 31.8 ±2.2 Ma (Vance and others, 1987). Vance and others (1987) have also suggested a correlation between these beds and the upper Ohanapecosh Formation, and for this reason the Wildcat Creek beds are not distinguished from the Ohanapecosh Formation in Figure 1.

FIFES PEAKS FORMATION

The Fifes Peaks Formation is a thick accumulation of basaltic andesite, andesite, rhyolite flows, tuffs, breccias, and laharic deposits (Schasse, 1987; Hammond and Hooper, 1991) that lies to the north of the Bumping Lake pluton. Fission-track ages on tuffs associated with Fifes Peaks lavas range from 22 to 26 Ma (Vance and others, 1987), while K-Ar dates range from 17 to 25 Ma (Hartman, 1973), which places this formation in the lower Miocene. Fifes Peaks volcano-caldera is a medium-sized stratovolcano composed chiefly of mafic andesite with a complex history of caldera formation and filling processes (Brunstad and Hammond, 1992).

COLUMBIA RIVER BASALT

Four to five flows of Grande Ronde Basalt, a formation of the Columbia River Basalt Group, occur to the east of the Bumping Lake pluton and lap on to the units described above (see Figure 1). These flows are aphyric to sparsely plagioclase-phyric tholeiitic flood lavas aged between 15.6 and 16.5 Ma (Watkins and Baksi, 1974; Lux, 1981; Long and Duncan, 1983; Schasse, 1987). Locally, the flows are interbedded with feldspathic sandstone or Ellensburg volcanic sedimentary rocks (Hammond and Hooper, 1991).

YOUNG INTRUSIONS AND FLOWS

Young porphyritic intrusive rocks with andesitic to dacitic geochemical signatures commonly cut the pluton in the Miners Ridge area. A rhyolite porphyry intrusion cuts the pluton at American Ridge in the northern region.

Two 140,000-730,000 yr. (Abbott, 1953; Clayton, 1983; Simmons and others, 1983; Schasse, 1987) andesite flows, referred to as andesite of Deep Creek, vented through Miners Ridge (Figure 2). The vent of the southern flow of the Deep Creek andesite forms a dome located directly south of Granite Lake. The lava flowed into the Deep Creek valley and continued for approximately three kilometers down the valley toward Bumping Lake. Since remnants of the flow can be found over 100 m up the north slope of Pear Butte Ridge, the flow probably existed before the Hayden Creek glaciation of the Deep Creek valley. The northern flow vented near the crest of Miners Ridge and flowed down its northern slope. This flow terminates at the shore of Bumping Lake, and

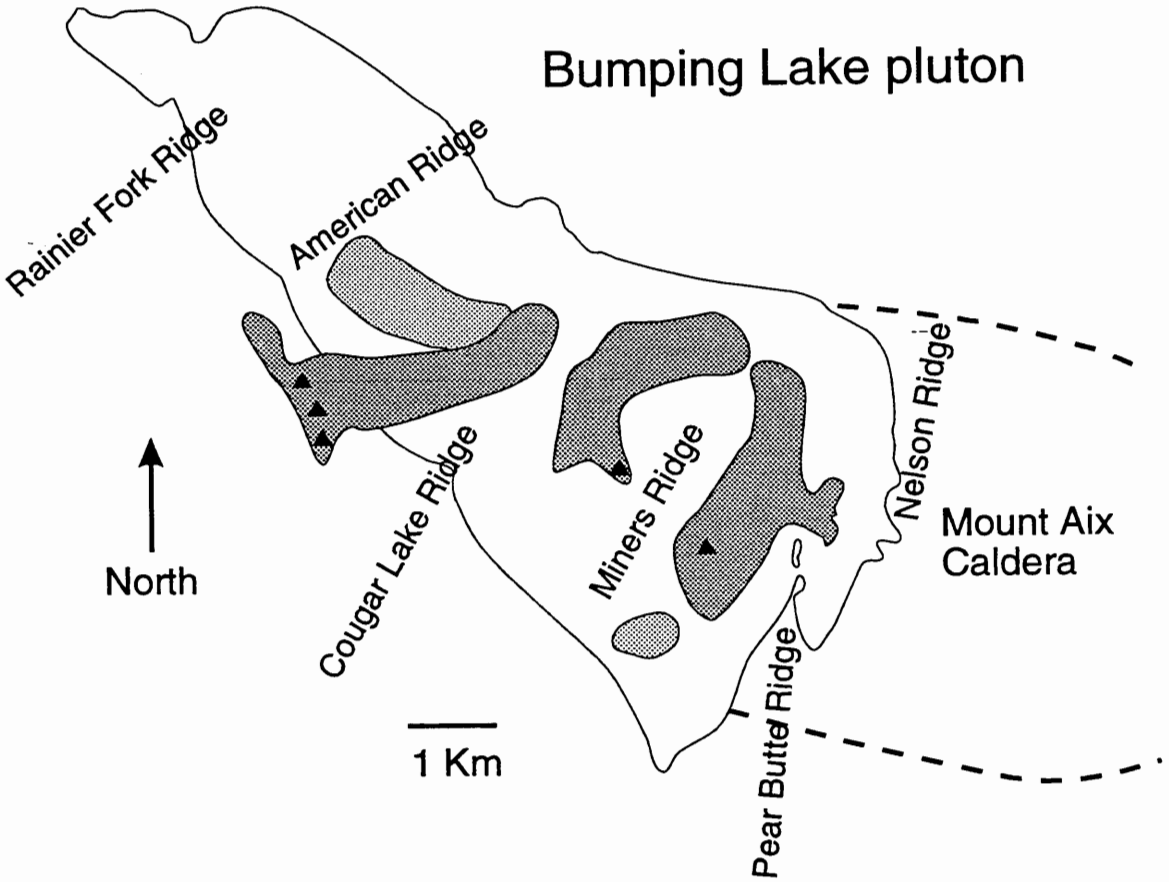

Figure 2. Simplified geologic map of the Bumping Lake pluton. Triangles represent Quaternary vents, and dark gray units represent lava flows from these vents. Light gray units are intrusions younger than the Bumping Lake pluton. For a detailed map on a topographic base, refer to Figure 3.

has reversed magnetic polarity (Abbott, 1953; Clayton, 1983), which places it older than about 780 ka.

REGIONAL STRUCTURES

A regional eastward homocline occurs between the Rimrock Lake inlier and Fifes Peaks (Figure 1). Arc strata and Columbia River basalt flows are deformed and exposed in this 20-35°E-dipping homocline (Hammond, 1989).

A set of northwest-striking folds enters the area from the northwest. One of these folds, the Chinook Pass anticline, is 15 km wide with 500 m amplitude. The fold axis of this anticline is terminated by the Bumping Lake pluton, which is elongated in the direction of the anticline. The eastern flank of this anticline is part of the regional eastward homocline described above. To the west, the Chinook Pass anticline is flanked by the shallow Yakima Peak syncline, which deforms rocks of similar age.

A set of southwest-striking folds less developed than the northwest-striking folds occur in the region also. These folds occur west of the Olympic-Wallowa lineament (OWL) and plunge northeast, roughly normal to the OWL. Strata as young as the Columbia River basalts are deformed by these folds. The Bethel Ridge anticline stretches west to east north of Tieton volcano (Swanson, 1966, 1978). A syncline lies to the north of the Bethel Ridge anticline that starts between the Mount Aix caldera and Edgar Rock volcano and extends south of the anticline located south of the Bumping River. A narrow syncline paralleled by a fault extends southeasterly along the Bumping River, possibly to the Mount Aix caldera.

CHARACTERISTICS OF THE PLUTON

The shallowly emplaced, predominantly granitic Bumping Lake pluton (BLP) is located approximately 35 km east of Mount Rainier. It extends 16 km from the Mount Aix caldera in the southeast to 1.5 km east of Chinook Pass in the northwest (see Figure 1). At its maximum, the pluton has a width of eight kilometers across Bumping Lake. The area of the pluton is about 120 km^2, which surpasses the minimum size requirement to be considered a batholith (Bates and Jackson, 1986). Only one date of the pluton has been reported: a zircon fission-track date of 24.7±0.6 Ma, which was obtained from the granite facies on Miners Ridge (Clayton, 1983). The Bumping Lake pluton is significant because it is one of only two large, epizonal, granitic intrusions presently exposed in the Cascade Range. The other is the 48 Ma Golden Horn batholith in the North Cascades (Tabor and others, 1968).

DISTRIBUTION OF ROCK TYPES IN THE PLUTON

Approximately 90% of the pluton's outcrop expression is granite, 9% granodiorite to quartz diorite, and the remaining 1% is a fine-grained, mafic-poor granite that occurs in dike and sill swarms cutting the granite.

Transitions from granite to granodiorite to quartz diorite are texturally and mineralogically gradational. In outcrop, granodiorite and quartz diorite occur only in two isolated areas, the first in the northwest at Highway 410 and the second in the southeast

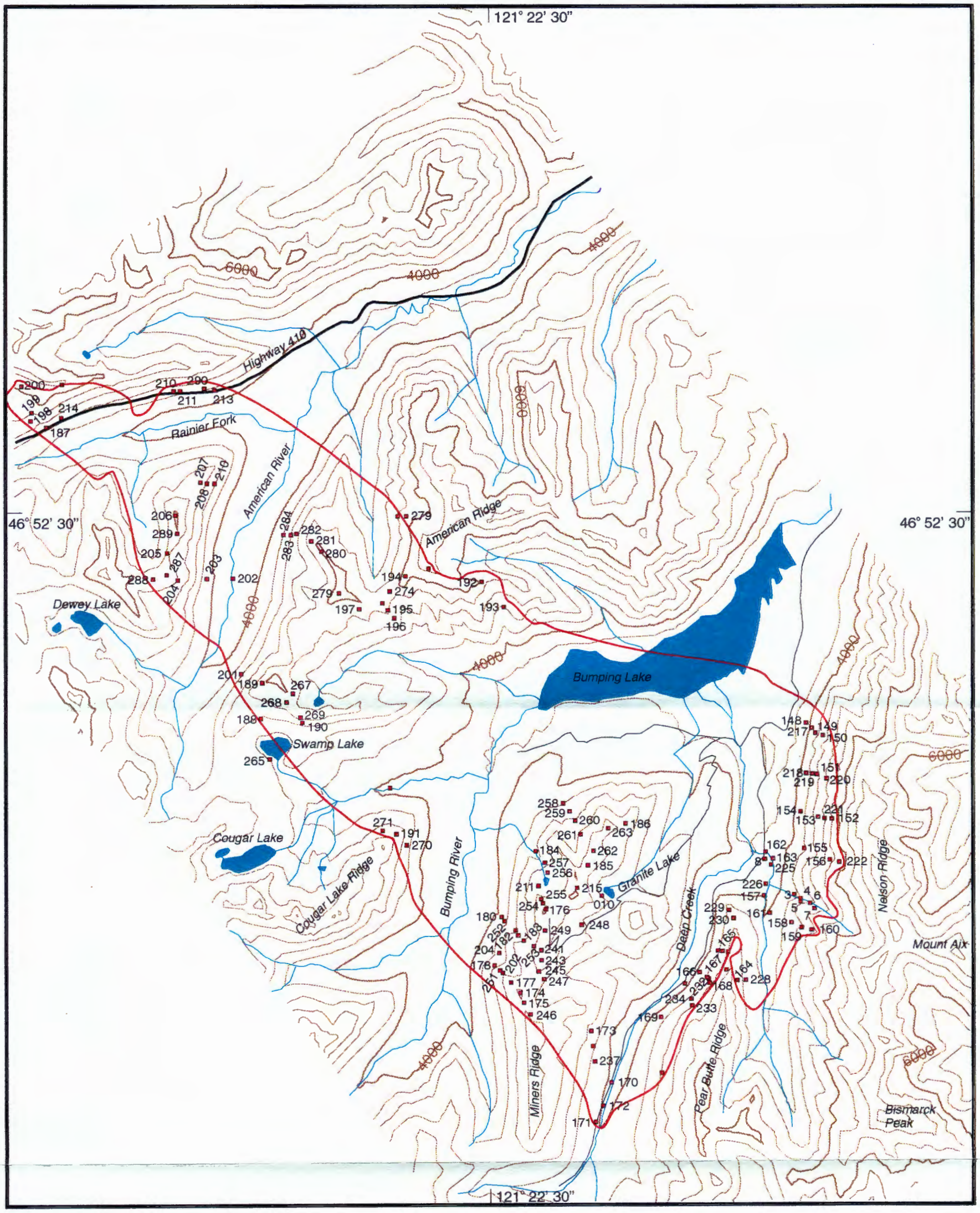

EXPLANATION

- Sample location
- Intrusive contact
- Roads
- Contour interval 400 feet

1 Mile

1 Kilometer

North

Mag. North

20°

Figure 3. Sample location map. Samples analyzed by XRF and ICP-MS are represented by red squares. Refer to Appendices A and B for UTM coordinates and chemistry of samples.

on Nelson Ridge. The pluton lacks a continuous mafic rim typically found in zoned plutons (e.g., Pankhurst, 1979; Stephens and Halliday, 1979; Fourcade and Allegre, 1981; Stephens, 1992). Trends in major and trace element chemistry with respect to SiO_2 show no significant compositional gap between quartz diorite, granodiorite, and granite (see Figures 5-11).

Petrography

Textures in the granite facies range from coarse-grained and porphyritic (quartz phenocrysts up to one cm) to medium-grained and equigranular; myrmekite is common through the range of textures. Essential minerals include quartz, plagioclase, K-feldspar, and biotite. Granodiorite may be distinguished from granite only by its lower K-feldspar content. Quartz diorite is almost exclusively limited to Nelson Ridge, and is characterized by its medium gray color, abundance of plagioclase, and lack of quartz. The fine-grained granite is white and commonly has 3-5 mm quartz phenocrysts. In general, the granite of the Bumping Lake pluton is texturally distinct from the fine- to medium-grained, equigranular texture common in the Tatoosh-White River pluton (Fiske and others, 1963; Murphy and Marsh, 1993), Spirit Lake pluton (Evarts and others, 1987), and Snoqualmie batholith (Erikson, 1969). Alignment of minerals is absent except near the intrusive contact where the pluton fills fractures in xenoliths.

Granite

Although textures in the granite facies vary widely, mineral content varies little. Five thin sections from the granite facies were examined in thin section and represent the

spectrum of textural characteristics. Sample 160 (sample locations shown in Figure 3) has 30% quartz, 30-35% plagioclase, 20-30% K-feldspar, 5% biotite, and 1% opaque minerals (Table I summarizes the modal abundances of the facies). The quartz is generally one millimeter in size, but occurs also as phenocrysts up to three millimeters. A myrmekitic texture occurs when quartz shares a crystal face with K-feldspar. The K-feldspar fills pore spaces between sub- and euhedral quartz and plagioclase indicating it crystallized late in the cooling history. Biotite is also a late-stage mineral and is most commonly associated with K-feldspar.

TABLE I

SUMMARY OF PETROGRAPHIC DESCRIPTIONS

Facies	Phenocrysts	Groundmass	Accessories
Fine granite	Plagioclase	Quartz, plagioclase, K-feldspar	
Granite	Quartz, plagioclase	Quartz, plagioclase, K-feldspar, biotite	Zircon, apatite, opaques
Granodiorite	Plagioclase	Quartz, plagioclase, K-feldspar, biotite, hornblende	Zircon, apatite, opaques
Quartz diorite	Plagioclase	Quartz, plagioclase, hornblende	Apatite, opaques

Sample 161 has 30% quartz, 45% plagioclase, 20% K-feldspar, 5% biotite, and <1% opaque minerals. Quartz is anhedral, 3-4 mm in size with incipient, poorly developed myrmekite when adjacent to K-feldspar. Plagioclase is strongly concentrically zoned in many grains such that the microscope stage rotates up to 55° as the extinction front passes from the core to the rim of the crystal. Most grains show albite twinning, are

anhedral, and about three millimeters in size. K-feldspar usually occurs in late-stage crystallization and less commonly as one millimeter, euhedral inclusions in quartz. Anhedral biotite occurs randomly. Part of a xenolith is included in the thin section. The xenolith is made up of 70% plagioclase and 30% biotite. No unusual textures or minerals occur at the granite-xenolith contact, nor do grain sizes change with distance from the contact.

Sample 178 is characterized by its large crystal sizes. The sample is made up of 35% quartz, 25% plagioclase, 30% K-feldspar, and 5-10% biotite. Opaque minerals make up much less than 1%. Quartz grains can be ~10 mm as phenocrysts, but are usually about five millimeters in size. Myrmekite is absent between quartz and K-feldspar. K-feldspar is averages five millimeters in size, anhedral, and commonly coarsely perthitic. Plagioclase is 4-6 mm, usually albite twinned, and occasionally concentrically zoned. Biotite is 3-4 mm and associated with K-feldspar. Small (<1 mm) zircon grains are common inclusions in biotite.

Sample 210 is comprised of 35% quartz, 35% plagioclase, 25% K-feldspar, 5% biotite, and trace opaques and zircon. Myrmekite, whose origin is uncertain but believed to be secondary (Best, 1982), is absent from this sample. K-feldspar is anhedral and late-stage. The crystals are perthitic and associated with biotite. Plagioclase ranges from anhedral to euhedral, and may be albite twinned and/or concentrically zoned. Biotite is also late-stage, and contains zircon inclusions.

Sample 207 has the most striking texture of all the thin sections. The sample is comprised of 30% quartz, 35% plagioclase, 25% K-feldspar, 5% biotite, 2-3% hornblende, and trace opaque minerals. Three distinct grain sizes exist in this sample: the

smallest is about 0.1 mm, the middle size is about one millimeter, and the largest crystals are average five millimeters. Plagioclase of the 0.1 mm size class are abundant and scattered evenly throughout the sample, but are not optically aligned. Glomerocrysts have been formed by the aggregation of the one millimeter plagioclase, which are concentrically zoned and contain inclusions of the 0.1 mm plagioclase. Plagioclase phenocrysts are five millimeters in size and are albite twinned with no inclusions. Quartz occurs in two forms: i) as five millimeter crystals with an inclusion free core measuring 1-2 mm in diameter and a two millimeter thick inclusion rich rim where the inclusions comprise about 50% of the volume, and ii) as 3-4 mm poikilitic crystals with abundant plagioclase inclusions (i.e., they have no pure quartz core). This implies that the small plagioclase laths were introduced into the melt after quartz had begun crystallizing. Poikilitic K-feldspar is mostly in the one millimeter size range with 0.1 mm inclusions of plagioclase and biotite. The K-feldspar is anhedral and perthitic. Some of the K-feldspar is surrounded by a thin reaction rim of plagioclase. Biotite is anhedral and occurs mostly in the 0.1 mm size range, but reaches up to 0.7 mm. It is associated with K-feldspar and opaque minerals. Hornblende occurs exclusively in the 0.1 mm size class, and is partly to wholly replaced by biotite.

Fine Granite

The fine granite facies is characterized by its fine grain size and lack of both biotite and hornblende. Sample 195 has 45% quartz, 45% K-feldspar, 10% plagioclase, and trace opaques and zircon. Quartz is subhedral and ranges from 0.1-0.5 mm in size, but is

generally 0.3-0.4 mm. K-feldspar ranges from 0.3-1.0 mm and is anhedral. Plagioclase occurs both as ~0.5 mm albite twinned crystals and 3-4 mm phenocrysts.

Granodiorite

Although not as abundant as granite, textures in the granodiorite facies also vary considerably. Sample 206 was taken from an outcrop near sample 207 and has a texture that is gradational between sample 207 and the granite described above. Its mineralogy consists of 20% quartz, 60% plagioclase, 15% K-feldspar, 3% biotite, 3% hornblende, and trace opaques. Anhedral quartz is commonly 1-2 mm in size, and occurs as 0.2 mm interstitial grains associated with K-feldspar. The mineral forms rare 3-4 mm phenocrysts, and where these occur, they have inclusions of K-feldspar. These inclusions fill fractures in the quartz instead of being euhedral in form. Generally, K-feldspar is not as coarsely perthitic as sample 207, and is less common. K-feldspar is associated with quartz, and is usually 1-2 mm in size, but also occurs as 0.1 mm interstitial grains. Biotite and hornblende commonly are found as inclusions. Plagioclase occurs in two distinct sizes. The smaller sized crystals are needle-like, 0.1-0.2 mm laths which make up the bulk of the groundmass. The larger sized crystals are concentrically zoned and are 3-4 mm in size. All plagioclase phenocrysts have a 0.1-0.2 mm thick plagioclase rim that is not optically aligned with the rest of the phenocryst and truncates albite twins. Biotite is less abundant than in sample 207. It is approximately 0.5 mm in size and interstitial. Hornblende in this sample is not being replaced by biotite as in sample 207, and is also about 0.5 mm in size and interstitial.

Sample 166 has 35% quartz, 55% plagioclase, 5% K-feldspar, 5% hornblende, <1% biotite, and <1% opaque minerals. 90% of the quartz occurs as 0.5-1 mm subhedral grains. The remaining 10% of the quartz is 2-3 mm phenocrysts associated with K-feldspar. These grain boundaries have an incipient myrmekitic texture. K-feldspar occurs as intergranular, late-stage, anhedral grains. The crystals are <0.5 mm and uncommon where the sample is dominated by plagioclase. Plagioclase occurs as sub- to euhedral two millimeters phenocrysts that are free of inclusions. The crystals are concentrically zoned and/or albite twinned. Hornblende is intergranular, anhedral, and late-stage. The crystals average 0.5 mm in size and are associated with plagioclase and quartz. A possible explanation for the difference in textures in this facies is that the range in texture is a result of the complex cooling history of a long-lived, periodically tapped magma body.

Quartz Diorite

Quartz diorite is characterized by its lack of K-feldspar and relatively low quartz content. Sample 156, for example, is 80% plagioclase, 8-10% quartz, 8-10% biotite, 1-3% hornblende, with trace opaque minerals. Plagioclase occurs both as five millimeter sub- to euhedral phenocrysts, but more commonly as an- to subhedral 2-3 mm groundmass. Concentric zoning is common as is albite twinning. Occasionally, the crystal is embayed and filled with biotite. Biotite is anhedral an interstitial. Secondary alteration has replaced some biotite rims with chlorite. Quartz is also anhedral and interstitial. Hornblende occurs associated with biotite and is late forming.

CLASSIFICATION

Representative samples from the different facies are plotted using the IUGS classification scheme. The results show that the main facies is a true granite. The pluton is also peraluminous (Figure 4) although minerals common in peraluminous granites such as muscovite, cordierite, andalusite, sillimanite, and garnet are absent.

Because the Bumping Lake pluton is located in the Cascade arc, it would be expected to be an I-type granitoid. However, the pluton straddles the boundaries between the I-type and S-type granitoids (Table II). The pluton has characteristics of both granitoid types, indicating that the source rocks are both igneous and sedimentary. The source

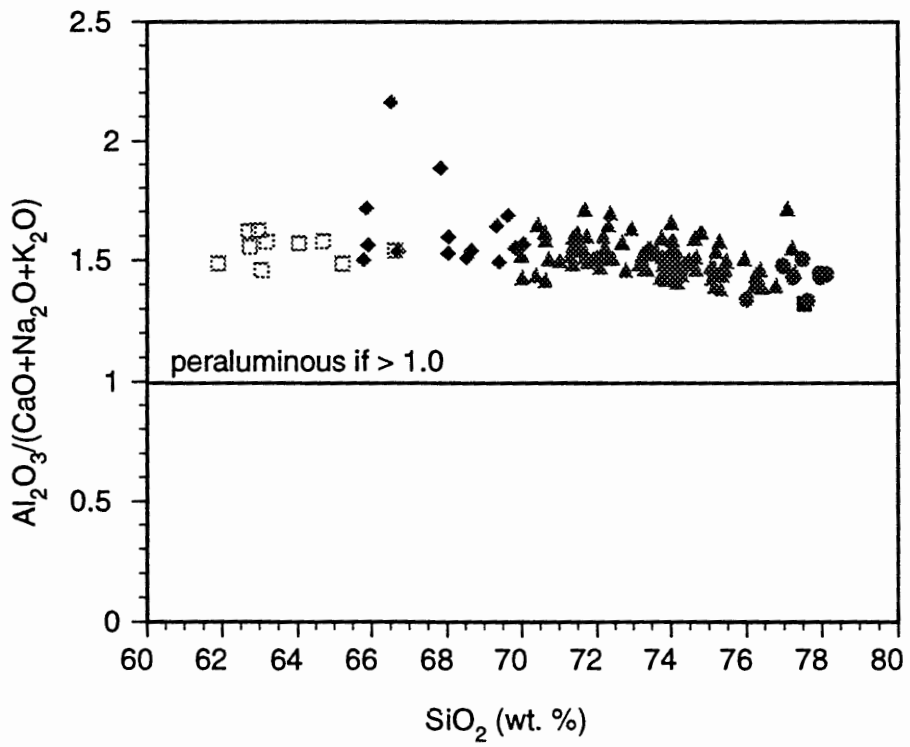

Figure 4. $Al_2O_3/(CaO+Na_2O+K_2O)$ vs. SiO_2. Because all facies of the pluton have A/CNK values >1, they are defined as peraluminous. Aphanite shown as closed squares, fine granite as closed circles, granite as closed triangles, granodiorite and closed diamonds, and quartz diorite as open squares.

region for most I-type granites is the deep crust (Clarke, 1992), which is likely heterogeneous (Miller and others, 1987). Southeast of the pluton, the pre-Tertiary basement, taken as a whole, is a tectonic melange of metasedimentary and metavolcanic rocks (Miller, 1985), which projects beneath the study area. A similar phenomenon exists in the Criffell pluton, Scotland, where the pluton has both I- and S-type characteristics with a basement of metavolcanics and metasediments (Stephens, 1992).

TABLE II

COMPARISON OF BUMPING LAKE PLUTON AND I- AND S-TYPE GRANITOIDS. DEFINITIONS AFTER CHAPPELL AND WHITE (1984), CHAPPELL AND WHITE (1992), AND NORMAN AND OTHERS (1992).

I-type	S-type	Bumping Lake pluton
relatively high sodium, Na2O normally >3.2% in felsic varieties, decreasing to >2.2% in more mafic types	relatively low sodium, Na2O normally < 3.2% with approx. 5% K2O, decreasing to < 2.2% in rocks with approx. 2% K2O	average weight percent Na2O is 3.93
Mol Al2O3(Na2O + K2O + CaO) < 1.1	Mol Al2O3(Na2O + K2O + CaO) > 1.1	1.51 wt. % A/NKC and 1.18 cation %
CIPW normative diopside or < 1% normative corundum	>1% normative corundum	normative corundum ranges from 0 to 4.9% and averages 0.53%
broad spectrum of compositions from felsic to mafic	relatively restricted in composition to high SiO2 types	weight percent SiO2 ranges from 62.9 to 78.1
regular inter-element variations within plutons; linear or near-linear variation diagrams	variation diagrams more irregular	linear to near-linear variation diagrams
hornblende common in more mafic rocks, and generally present in felsic varieties	hornblende absent, muscovite common, biotite common and up to 35% of rock	hornblende common in quartz diorite, but absent in granite
apatite inclusions common in biotite and hornblende	apatite occurs in larger discrete crystals	apatite uncommon, but exist as inclusions in biotite

CONVECTION

In some magma chambers, viscosity has been shown to be an important process that effects a wide range of physical processes such as magma withdrawal (Spera and others, 1986), melt transport phenomena (Petford and others, 1993), chemical fractionation

(Spera and others, 1982), and chemical zonation (Marsh, 1989). It is the purpose of this section to demonstrate that viscosity plays a fundamental role in determining whether convection can be initiated and maintained in a siliceous magma chamber.

Viscosity is defined as the ratio of shear stress to strain rate. A good approximation for a melt's viscosity may be obtained from major element chemical data using a BASIC program by McBirney and Murase (1984). Using this program, the log of the effective viscosity of the Bumping Lake pluton at 900°C with one millimeter quartz phenocrysts is 10.196 Poise, which is used below in the calculation of the Rayleigh number.

A magma chamber will cool by conduction until the difference in temperature between the part of the chamber that is dissipating heat (assumed to be the chamber roof) and the part of the chamber that is hottest (assumed to be the floor where basalt is injected) reaches a critical value. Assuming Rayleigh-Benard convection, once this critical temperature difference is reached, convection begins. A critical value of the Rayleigh number, Ra_c, corresponds to the onset of convection, which typically ranges from 500-2000 (Marsh, 1989). The Rayleigh number is defined as,

$$Ra = \frac{\alpha g \Delta T l^3}{\eta K}$$

where α is the coefficient of thermal expansion, g is gravitational acceleration, ΔT is the temperature difference, l is length, η is kinematic viscosity, and K is thermal diffusivity. For a given magma chamber, the melt composition has a large effect on Ra_c because rhyolitic melts are 5-10 orders of magnitude more viscous than basaltic melts. Magmas with

values of Ra ~10^{15}-10^{20} convect vigorously (Spera, 1980), while magmas with values of Ra ~10^{4} probably do not convect at all (Marsh, 1989).

Simplifying the emplacement process of the Bumping Lake pluton by assuming thermal homogeneity at the time of emplacement allows an approximation of a possible post-emplacement evolutionary path. Immediately following emplacement, the pluton cooled by conduction until the thermal difference between the top and bottom of the pluton reached Ra_c. Because a temperature difference of only 1°C would have been required for the initiation of convection, the magma probably began to convect immediately after emplacement. Ignoring the increase in viscosity due to crystallization and assuming the base of the chamber had a temperature of about 1200°C (based on temperatures of molten basalt) and the top of the chamber had a temperature of about 850°C (based on Hildreth, 1980), Ra reached a maximum of about 10^{7}. This value falls below the range of vigorous convection described by Spera (1980), and suggests that convection in the Bumping Lake pluton, although existent, was weak. If an increase in viscosity with crystallization is factored in, Ra will decrease and therefore decrease the likelihood that the melt convected.

This interpretation can be verified by calculating the Reynolds number, Re, of the magma, which is a measure of a liquid's turbulence and is defined as,

$$\mathrm{Re} = \frac{\rho v l}{\eta}$$

where ρ is density, v is velocity, l is the length of the chamber, and η is the viscosity of the fluid. Less viscous melts such as basalt and basaltic andesite have large

Reynolds numbers and as a result can convect turbulently. Compared to mafic melts, felsic melts are slightly less dense and have viscosities generally 10^5 to 10^{10} times greater and therefore lower velocities. Using the parameters calculated for the Rayleigh number, the Re value for the Bumping Lake pluton is on order of 10^{-9}. Based on this value, convection could not have been turbulent and, as the Rayleigh number indicates, was more likely weak.

PETROGENESIS

Although commonly used in petrogenetic interpretation, variation diagrams have a number of shortcomings. As stated by Clarke (1992) these are: i) major elements suffer from the problem of closure, which make correlations between two elements appear better than they actually are (Chayes, 1960); ii) because variation diagrams are restricted in the number of variables that they show, each diagram must be considered as a small part of the whole, and many diagrams must be considered together to draw any conclusions about evolutionary history; and iii) perfect linear correlations are not always attributable to one cause, and deviations from a trend, although perhaps not understood, are nevertheless significant. However, when used in conjunction with field and petrologic data, variation diagrams can be a powerful tool. The approach of combining field, petrologic, and chemical data to make conclusions about petrogenesis is used in this study of the Bumping Lake pluton.

Strontium is strongly partitioned into plagioclase, and the Sr-CaO diagram confirms plagioclase fractionation (Figure 5). The correlation between Ba and Sr (Figure 6) demontrates the relationship of K-feldspar and plagioclase fractionation. An increase in Ba from the quartz diorite facies to the granite facies indicates that K-feldspar is not being removed with plagiocalse during the early stages of fractionation. A decrease in Ba from the granite facies to the highly fractionated fine granite facies indicates that K-feldspar is being fractionated in these facies. Petrography supports this fractionation history.

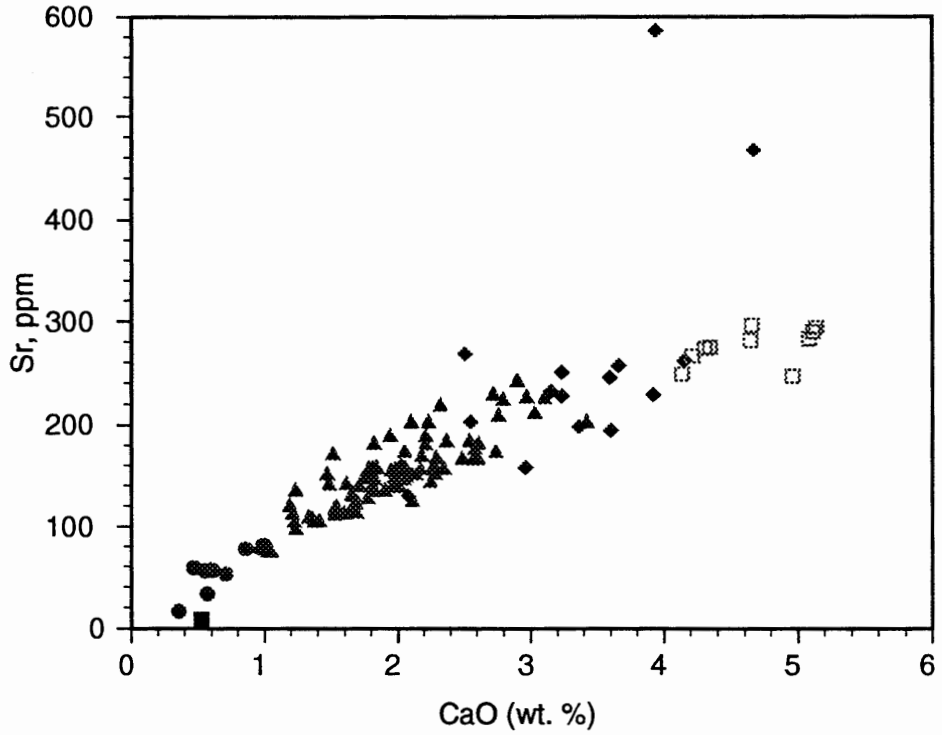

Figure 5. Sr vs. CaO. Sr is strongly partitioned into plagioclase, so a decrease in Sr with decreasing CaO indicates that plagioclase fractionation played an important role in the differentiation history of the pluton. Aphanite shown as closed squares, fine granite as closed circles, granite as closed triangles, granodiorite as closed diamonds, and quartz diorite as open squares.

K-feldspar grains are anhedral and therefore formed late in the crystallization sequence. The CaO-Na_2O-K_2O diagram suggests control of chemical evolution in the pluton by removal of plagioclase (Figure 7).

Zirconium is closely tied with differentiation and in the Bumping Lake pluton, decreases regularly in concentration as SiO_2 increases (Figure 8). TiO_2 shows a strong positive correlation with Zr (Figure 9), indicating that it also decreases with differentiation. Phosphorus is tied up principally in apatite and monazite, minerals that also appear to decrease modally with differentiation. P_2O_5 shows a very strong correlation with dif-

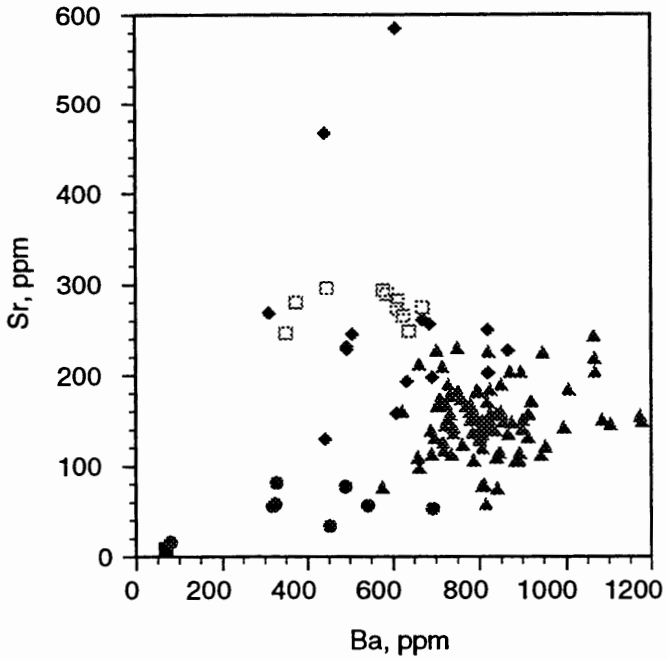

Figure 6. Sr vs. Ba. If K-feldspar continuously fractionated with plagioclase, then a linear correlation between Ba and Sr would exist. Here, Ba increases and then decreases as fractionation progresses. Symbols as in Figure 5.

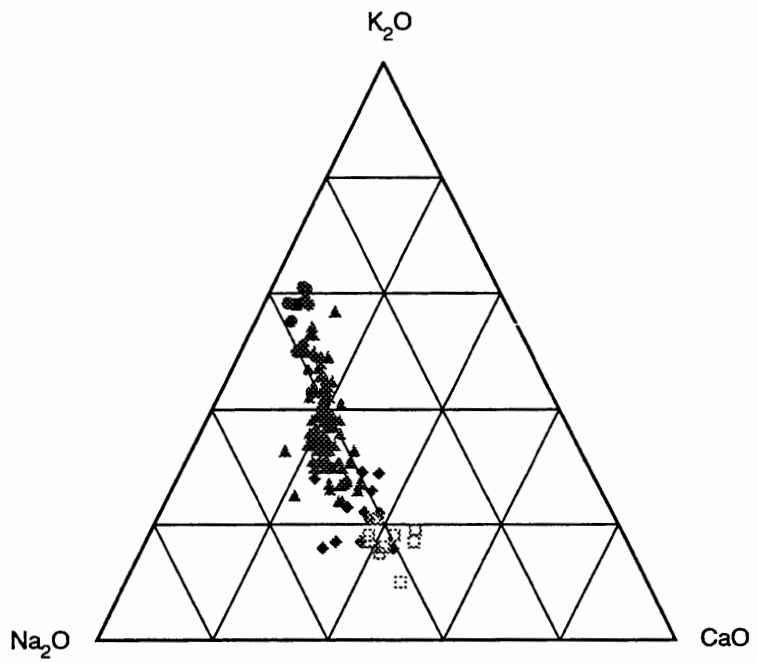

Figure 7. CNK ternary diagram. Shows that as differentiation progressed, the melt became progressively depleted in CaO and enriched in K_2O. This indicates the removal of plagioclase, and agrees with the pattern shown in Figure 5. Symbols as in Figure 5.

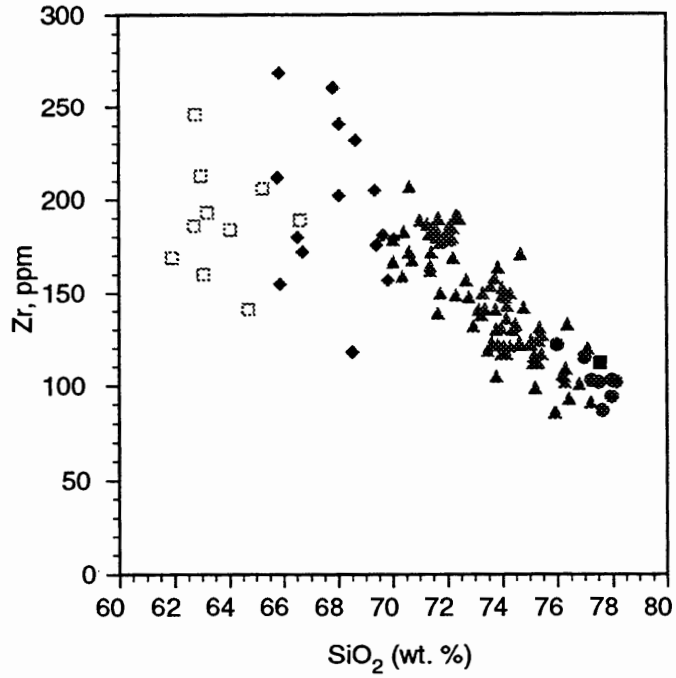

Figure 8. Zr vs. SiO_2. Plot showing a decrease in Zr with increasing SiO_2. The scatter shown in the granodiorite and quartz diorite may be attributed to assimilation of host rocks. Symbols as in Figure 5.

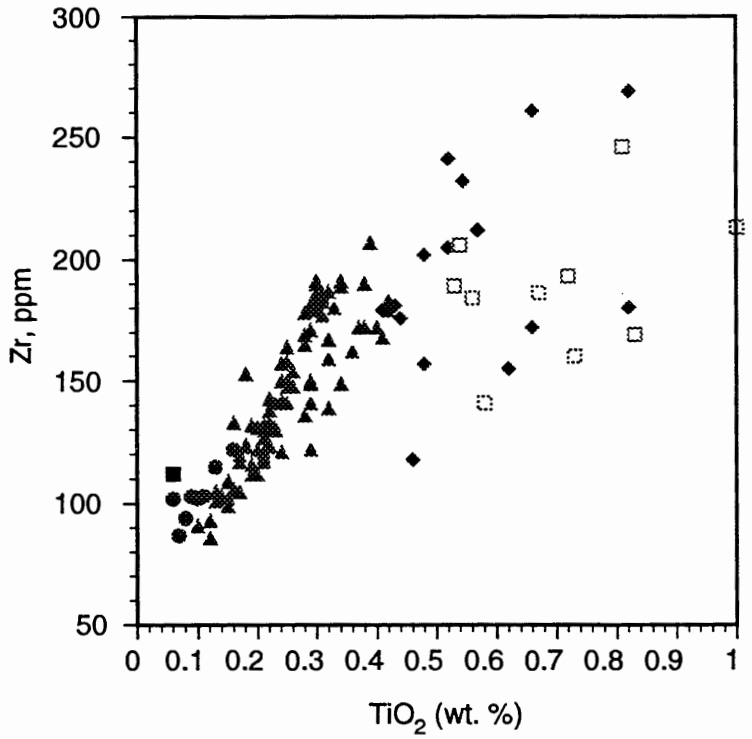

Figure 9. Zr vs. TiO_2. TiO_2 increases as Zr increases, which indicates that it decreases with differentiation. Symbols as in Figure 5.

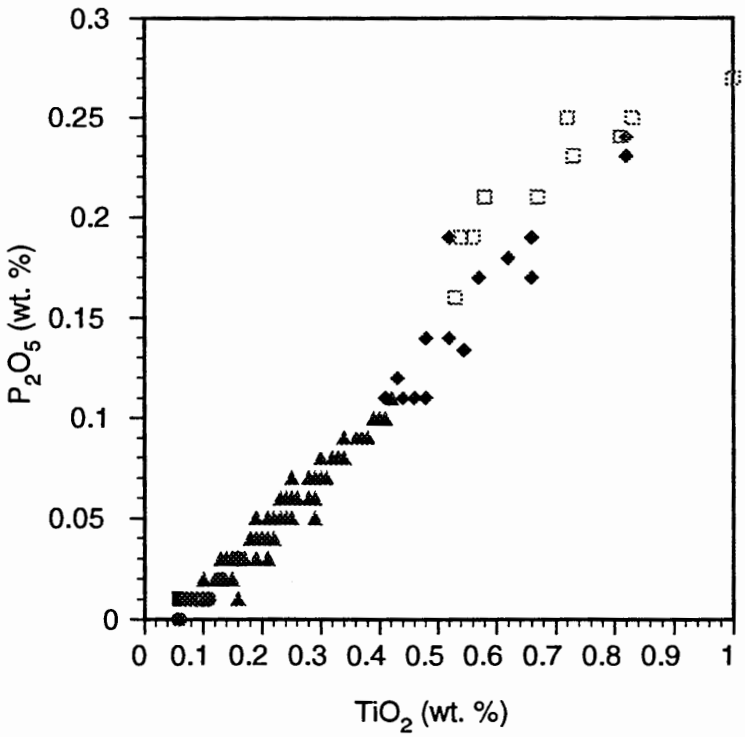

Figure 10. P_2O_5 vs. TiO_2. P_2O_5 shows a very strong correlation with TiO_2, which agrees with the observation that the accessory minerals apatite and monazite decreased modally with differentiation. Symbols as in Figure 5.

ferentiation (Figure 10), suggesting that its concentration is closely tied to crystal-liquid fractionation processes.

The plot that defines the pluton as peraluminous (Figure 4) also shows a slight decrease in excess alumina with differentiation. When SiO_2 is replaced with CaO on the x-axis (Figure 11) the trend remains, which indicates the presence of hydrous fluid phases and/or assimilation (Halliday and others, 1981). These possibilities may be further tested using K/Rb ratios. High K/Rb ratios are typical of magmatic processes and lower ratios can only be reached by fluid interaction effects (Clarke, 1992). A plot of K_20 vs. Rb (Figure 12) shows only high ratios, which indicates that assimilation, not fluid interaction, is responsible for the alumina trend. Evidence for assimilation is present in the field

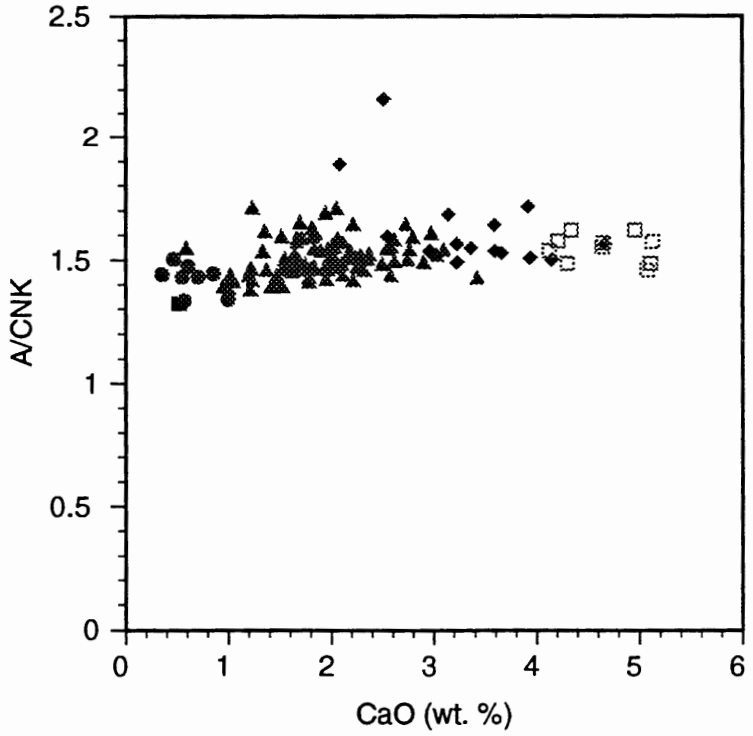

Figure 11. A/CNK vs. CaO. The slight decrease in excess alumina with decreasing CaO indicates assimilation. Vertical axis as in Figure 4. Symbols as in Figure 5.

as well. Near the intrusive contacts on Nelson Ridge and Highway 410, the pluton crystallized as it actively stoped pieces of country rock. Xenoliths of country rock are large and angular near the contact, but become smaller and more rounded with increasing depth (in some cases over 200 m) into the pluton. Assimilation of country rock may have been more or less continuous throughout the three million year life of the pluton (see Relationship to the Mount Aix caldera, below), and would be expected to effect the chemistry of the pluton.

Rare earth element (REE) patterns in the Bumping Lake pluton (Figure 13) are similar to those of other volcanic arc granites (Pearce and others, 1984). The slope of the chondrite-normalized REE patterns changes from negative in the light rare earth elements (LREE) to nearly flat in the heavy rare earth elements (HREE). As differentiation pro-

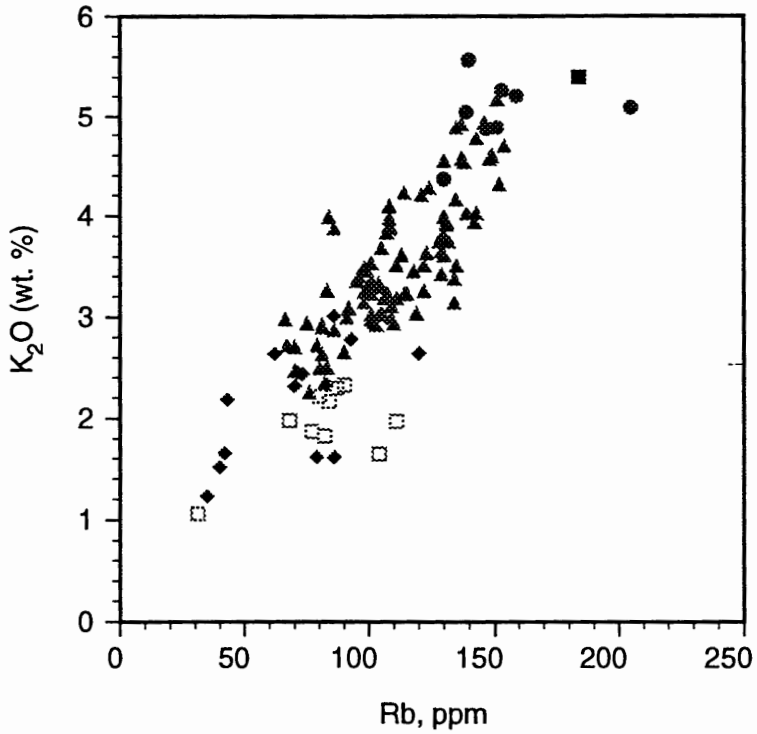

Figure 12. K_2O vs. Rb. High K/Rb ratios as shown here are achieved only by magmatic processes, which indicates that fluid interaction effects were minimal. Symbols as in Figure 5.

gressed in the pluton, LREE were depleted, a negative europium anomaly became more pronounced, and HREE showed no significant change. These trends are similar to those observed by Miller and Mittlefehldt (1982), who concluded that fractionation of LREE-rich accessories (e.g., allanite or monazite) is responsible for LREE depletion in highly felsic magmas. Accessory minerals tend to decrease in abundance with differentiation in the rocks of the Bumping Lake pluton, which supports the chemical evidence that fractionation of LREE-rich accessories occurred. Fractionation of feldspars is implied by the decrease in Eu/Eu* (observed Eu divided by Eu value predicted by drawing a straight line between the Sm and Gd values), which supports the evidence drawn from the variation diagrams in the previous section.

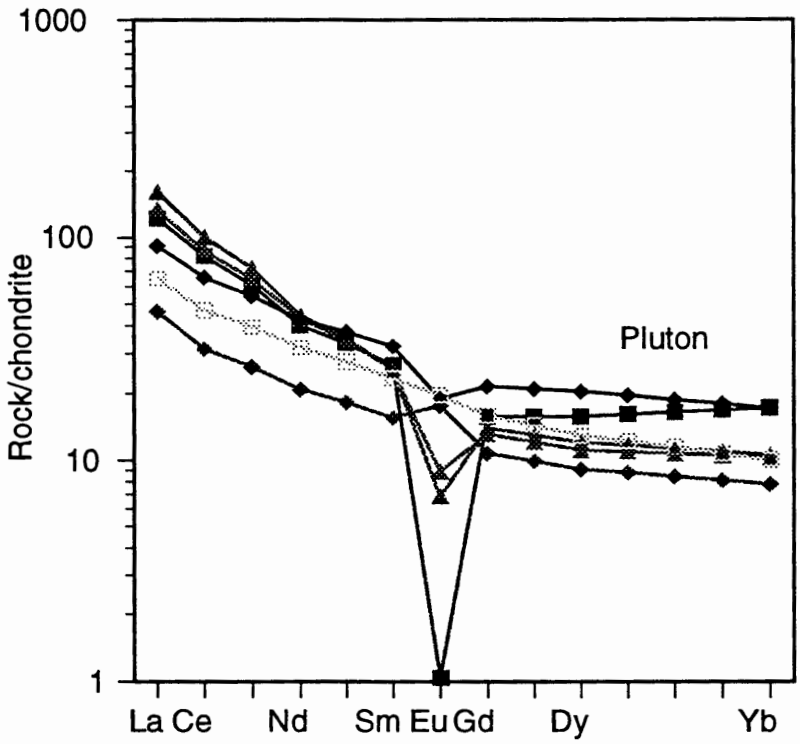

Figure 13. REE spider diagram for pluton samples. Note increase in Eu/Eu* value with differentiation. Symbols as in Figure 4. Normalization values after Nakamura (1974).

LATE-STAGE, HIGHLY FRACTIONATED LIQUIDS

In modeling externally cooled, crustal magma chambers, researchers have developed a framework for the fractionation of late stage, felsic magmas (e.g., Chen and Turner, 1980; Turner and Gustafson, 1981; Sparks and others, 1985; Nilson and others, 1985; Turner and Campbell, 1986). Field evidence has also been found in granitic plutons for these highly fractionated magmas (e.g., Boden, 1989; Mahood and Cornejo, 1992). The chemistry of the fine-grained granite facies of the Bumping Lake pluton indicates that it was a highly fractionated melt (Figures 5-11). This facies has the highest $Si0_2$, K_2O, and Rb content; the highest Rb/Zr, and Rb/Sr ratios; and the lowest TiO_2, MgO, P_2O_5, Zr, CaO, and Sr content, all of which indicate evolved composition.

In the field, the fine grained granite cuts the coarse grained granite and granodiorite, and occurs both as 10-30 cm thick tabular bodies and pods ranging from <1 to ~20 m but averaging 1-2 m in diameter. It is unknown whether these pods are discrete bodies or whether they extend some depth into the pluton. On Cougar Lake ridge, the bodies are tabular, horizontal, and spaced at ~25 m intervals. A sharp and even contact indicates that the fine granite was emplaced into the coarse granite when the coarse granite had cooled to the point of being brittle. The fine granite probably originated from deep within the pluton where temperatures were still high enough for the melt to be near the liquidus. The melt rose into the coarse granite and filled extensional fractures that existed as a result of cooling contraction, eruptive drawdown, fresh input of magma, faulting, or vapor saturation (Mahood and Cornejo, 1992). On Miners Ridge and Nelson Ridge, however, the fine granite occurs in irregularly shaped pods, which suggests that the host rock was ductile at the time it was intruded. Fine granites distributed throughout the pluton are chemically indistinguishable and were therefore emplaced at or near the same time. The differing contact relationships suggest that the pluton was molten in its southeastern extremity and mostly solid in the northwest at the time of emplacement. The pluton was more active physically and/or thermally for a longer period of time in the southeast.

SPACIAL VARIATIONS IN CHEMISTRY

Extensive sampling of the pluton revealed some consistent spacial chemical trends. Near the margins of the pluton, weight percent SiO_2 decreases with increasing elevation, and, therefore, with depth into the pluton (Figures 14 and 15), which is consistent

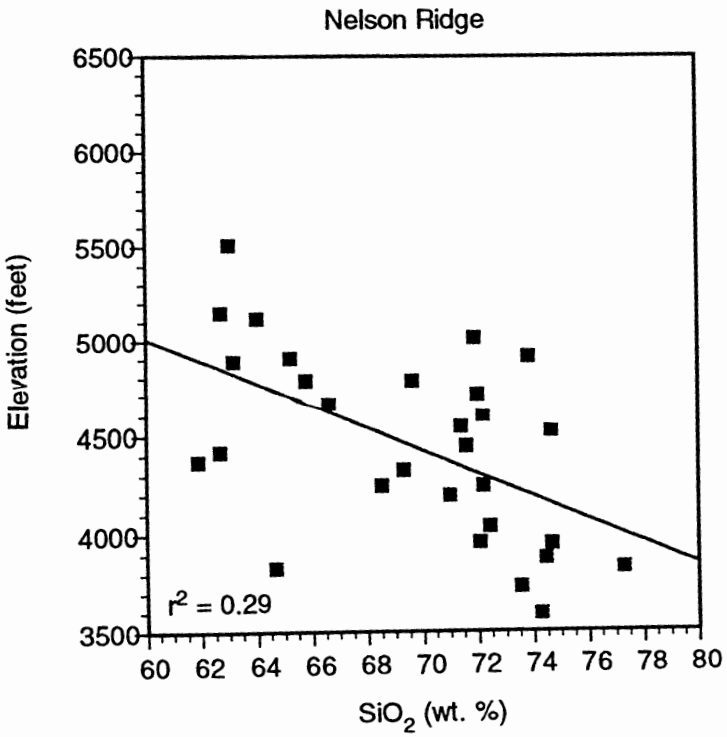

Figure 14. Elevation vs. SiO_2 in the granite facies on Nelson Ridge.

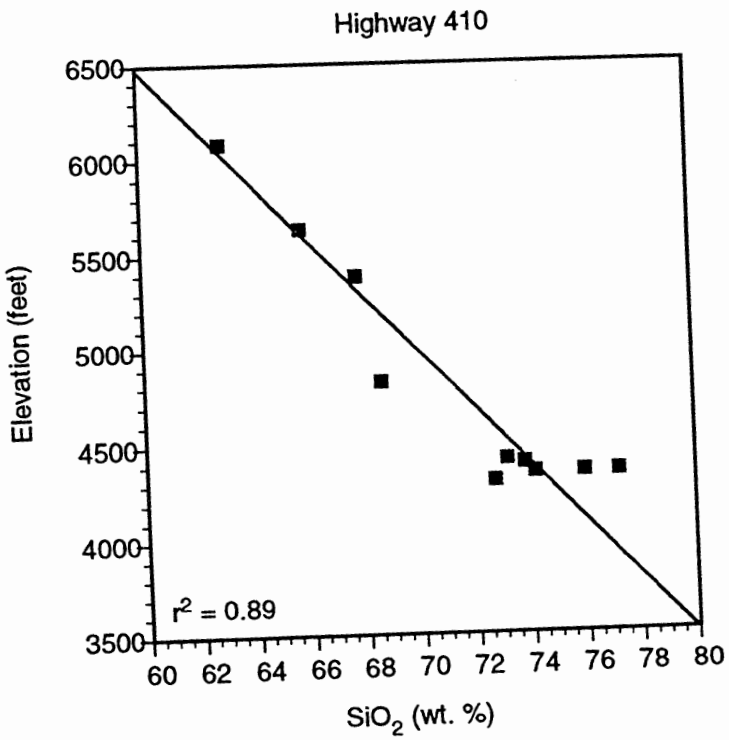

Figure 15. Elevation vs. SiO_2 in the granite facies near Highway 410.

with the interpretation that andesitic xenoliths were stoped and assimilated into the melt. Samples from Pear Butte Ridge show a weak positive correlation, but because of its low r^2 value (Table III), the correlation is probably not significant. Similarly, samples from American Ridge (Figure 16), Miners Ridge (Figure 17), and Rainier Fork Ridge have such low r^2 values that a variation in SiO_2 with respect to elevation does not exist. Since the intrusive contacts near these five locations are nearly vertical, the plutonic rock there probably represents a deeper level in the pluton where the effects of assimilation are not noticeable .

TABLE III

SUMMARY OF REGRESSION DATA FROM ELEVATION VS. SiO_2 CHARTS

Location	Slope of best fit line	r^2 value
American Ridge	5.58	0.0665
Highway 410	-6.68	0.89
Miners Ridge	-2.70	0.0062
Nelson Ridge	-5.80	0.29
Pear Butte Ridge	2.79	0.074
Rainier Fork Ridge	2.74	0.013

The regions of the pluton that show neither a consistent increase nor decrease in SiO_2 with elevation may indicate that i) the magma in that part of the chamber was disrupted, possibly by an eruption through a ring fault at the caldera margin; ii) the coarse granite facies did not undergo density stratification, a conclusion similar to Hildreth's (1981) of the Bishop Tuff magma chamber; iii) these areas have undergone varying degrees of silicification due to local mineralization. The third possibility may be ruled out on the basis that the abundance of mobile elements in samples taken from these regions

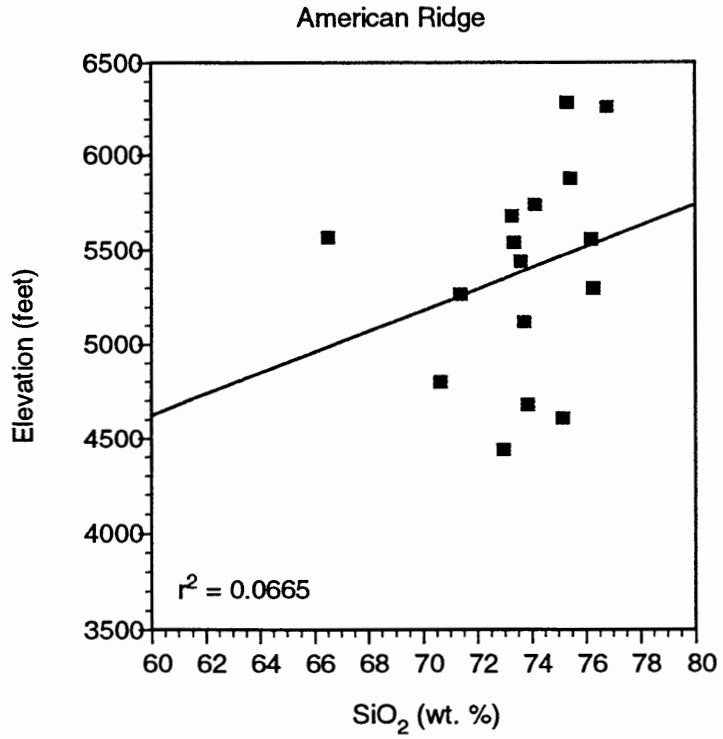

Figure 16. Elevation vs. SiO_2 in the granite facies on American Ridge.

are similar to samples from elsewhere in the pluton. It is likely that a combination of i) and ii) is responsible for the distribution pattern of SiO_2.

A useful diagram for the interpretation of spacial variations in chemistry is a contour diagram. In this diagram, contour lines connect areas with equal concentrations of a given element. In an SiO_2 contour diagram (Figure 18), the two areas of the pluton with granodiorite (Nelson Ridge and Highway 410) are represented by low SiO_2 values. Note the areas of relatively low SiO_2 to the north and south of American Ridge and the "high" at Miners Ridge. These areas correspond well with the spacial variation of Zr (Figure 19). Areas low in SiO_2 lows are high in Zr highs, and SiO_2 highs are Zr lows, which agrees with the trends defined in the Harker variation diagrams (see Figures 8-11). Figures 18 and 19 show that samples taken from Miners Ridge are highly differentiated.

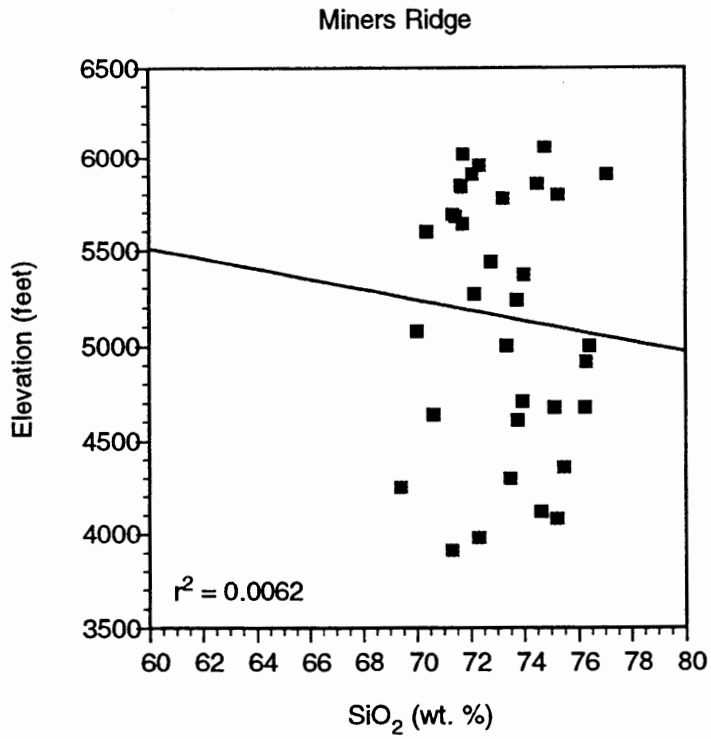

Figure 17. Elevation vs. SiO_2 in the granite facies on Miners Ridge.

Generally, as differentiation progresses, Zr decreases and Rb increases; therefore, the Rb/Zr ratio should vary systematically. In the case of the Bumping Lake pluton, the variation is not linear , and a two component plot is of little use. When Rb/Zr is plotted as a contour diagram, however, an interpretation is more straight forward (Figure 20). A high Rb/Zr ratio occurs on Miners Ridge at the same location as the Zr low and SiO_2 high, and two areas of low Rb/Zr also match the Zr and SiO_2 plots.

These irregularities may indicate different levels in the pluton. The less differentiated areas over American Ridge may represent a lower level in the pluton, which agrees with earlier interpretation of the significance of relatively highly differentiated rocks in this area. Conversely, the highly differentiated area over Miners Ridge may represent a relatively high level of the pluton.

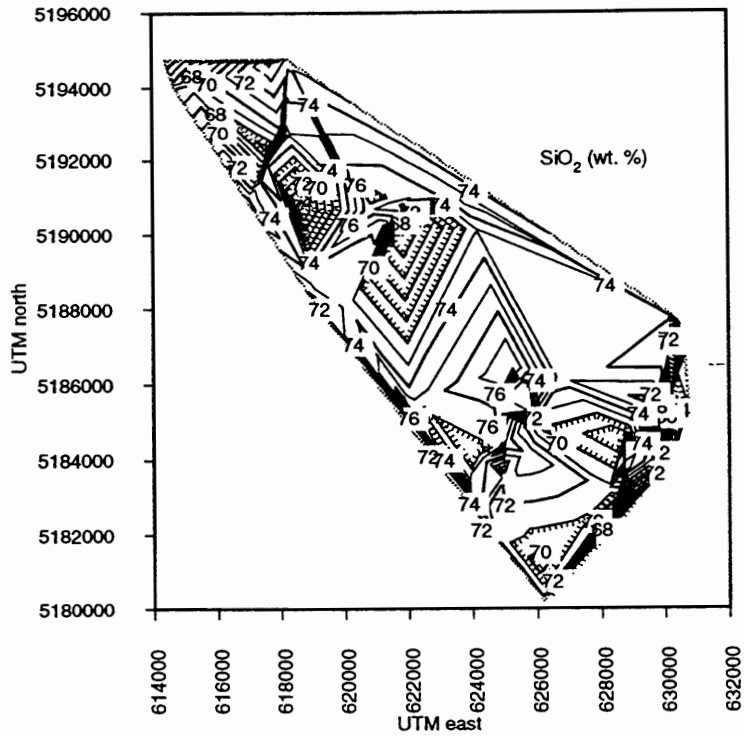

Figure 18. SiO_2 contour map of the granite facies.

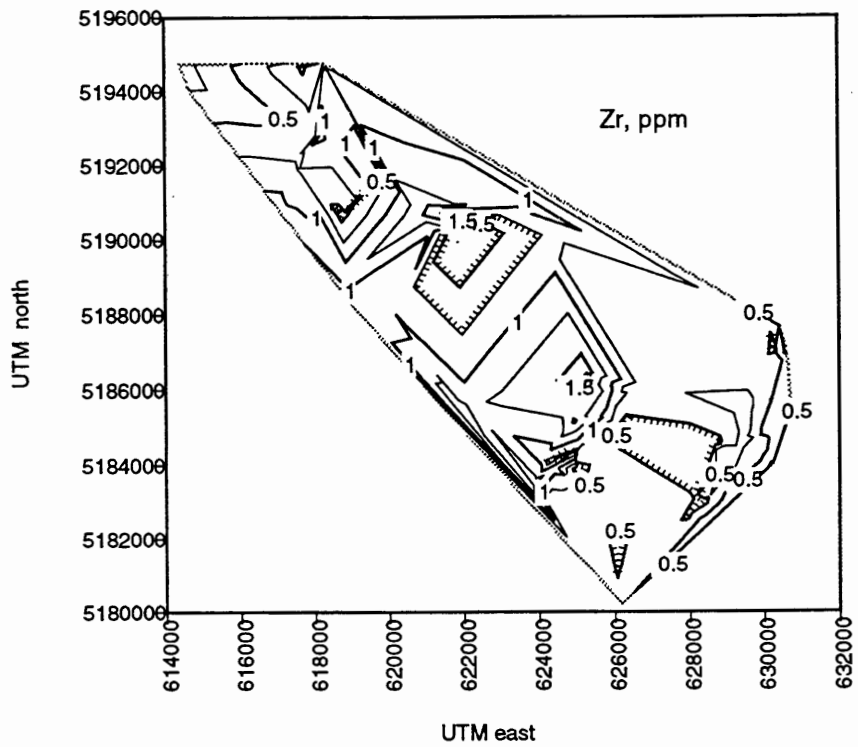

Figure 19. Zr contour map of the granite facies.

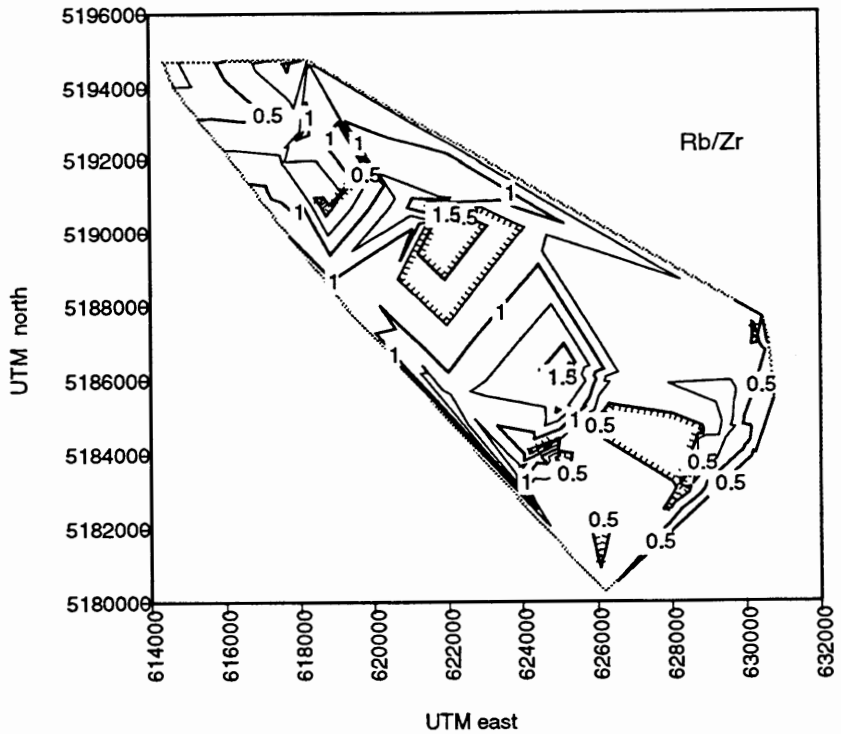

Figure 20. Rb/Zr contour map of the granite facies.

MINERALIZATION

Alteration due to the young andesite porphyry intrusion on Miners Ridge likely produced a zone of copper mineralization in the granite facies of Miners Ridge. Alteration in the BLP associated with the rhyolite intrusion on American Ridge was dated at 6.3±0.2 Ma (Armstrong and others, 1976) by K-Ar.

RELATIONSHIP TO MOUNT AIX CALDERA

The roof of the pluton at its southeast margin is flat, found half way up the western slope of Nelson Ridge, and possibly directly underlies collapse breccia from the caldera. This contact indicates that the pluton projects southeast beneath the Mount Aix caldera. The 28 Ma Bumping River tuff-north (BRTn), 25 Ma Bumping River tuff-east (BRTe), and 25 Ma Cash Prairie tuffs (CPT) (dates from Schreiber, 1981; Vance and others, 1987) are interpreted based on field criteria (Paul E. Hammond, pers. commun., 1994) to have been derived from the caldera. Because these tuffs are quartz-bearing and have a high wt. % SiO_2, their source must also have been highly siliceous. Paul. E. Hammond (pers. commun., 1994) estimates that the cumulative volume of the three tuffs erupted from the Mount Aix caldera exceeds 100 km^3, which suggests that an individual eruption was approximately as large as the caldera-forming eruption of Mt. Mazama, Oregon. A caldera typically empties about 10% of its chamber during an eruption (Smith, 1979); therefore, in addition to being highly siliceous, the Mount Aix caldera source must have had a large volume. In the region surrounding the caldera, the Bumping Lake pluton is an obvious and immediate suspect for being the source because it is large, predominantly granitic, a similar age, and is exposed directly beneath the caldera. The Bumping Lake pluton is the only realistic source because no other large, granitic, Oligocene pluton is known within 100 km of the caldera. Establishing a strong chemical and petrologic relationship between the pluton and the tuffs would clinch the argument.

CHEMICAL RELATIONSHIP

Because a three million year hiatus exists between the eruption of two of the three tuffs, a trace element that is effected by differentiation may chemically distinguish the tuffs. Zr is such an element in that it generally decreases with differentiation, and in this case clearly distinguishes the tuffs from each other. When Zr is plotted against SiO_2 (Figure 21), Zr appears to follow a normal differentiation trend within and between BRTn and CPT. These two tuffs fall directly on the fields defined by the pluton. BRTe has unusually high Zr for its SiO_2 values, which may indicate that it represents the least

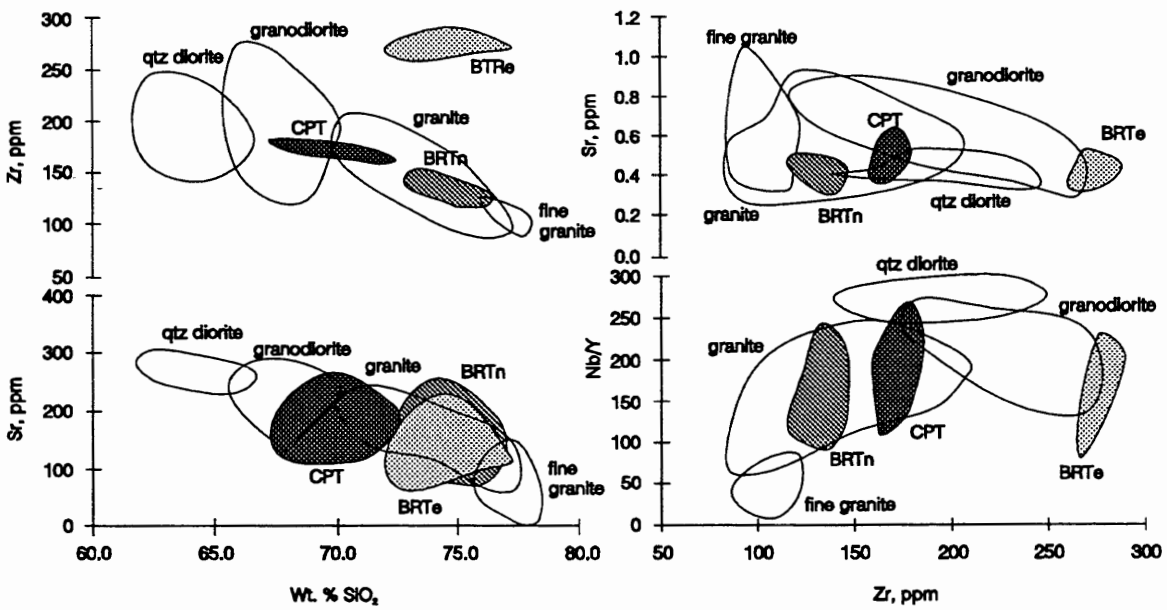

Figure 21. Chemistry of the Bumping River (BRTn and BRTe) and Cash Prairie tuffs (CPT). For comparison, facies from the pluton are also represented. Circles represent a field in which all samples of a particular facies or tuff plot.

differentiated, least evolved, and therefore oldest composition of the magma. BRTn and CPT match plutonic samples with more than just their Zr and SiO_2 values.

The chemistry of a tuff represents a "snapshot" of a magma chamber's chemistry, so tuffs such as BRTn, BRTe, and CPT may be compared with the pluton by defining a tuff in terms of a mean with a compositional range of two standard deviations. This approach does not suffer from the problems associated with two component variation diagrams because every major and minor element is considered. When the BRTn, BRTe, and CPT are compared to the pluton in this manner, 10 granite samples match BRTn and seven granite and two granodiorite samples match CPT with a 95% confidence interval (Table IV). The BRTe has no equivalent granite sample, but a plutonic equivalent may exist at depth.

TABLE IV

STATISTICAL CHEMICAL DATA OF THE TUFFS

	BRTn 2σ	BRTn -2σ	BRTe 2σ	BRTe -2σ	CPT 2σ	CPT -2σ
SiO2	76.89	72.65	78.90	71.05	73.69	67.29
Al2O3	14.86	12.90	14.60	13.57	16.78	14.19
TiO2	0.30	0.15	0.52	0.27	0.69	0.34
FeO*	3.20	1.77	4.67	0.00	5.37	1.95
MnO	0.10	0.00	0.10	0.00	0.13	0.00
CaO	4.71	1.00	4.01	2.16	3.93	1.78
MgO	0.73	0.00	1.04	0.00	1.39	0.16
K2O	4.55	1.20	2.91	0.92	3.93	1.80
Na2O	4.29	0.67	3.99	1.69	4.76	1.64
P2O5	0.05	0.01	0.10	0.00	0.14	0.05
Ni	14	6	14	8	19	5
Cr	12	0	11	0	18	2
Sc	11	0	18	2	17	7
V	33	0	145	0	83	32
Ba	983	310	862	74	976	486
Rb	136	29	78	35	146	54
Sr	350	0	275	16	263	93
Zr	151	117	292	254	182	155
Y	34.5	21.2	52.1	30.8	34.9	21.7
Nb	14	8	22	14	16	11
Ga	20	12	24	13	21	14
Cu	18	7	16	2	26	15
Zn	66	51	137	0	79	30
Pb	13	6	16	1	15	9
La	45	8	39	26	36	14
Ce	77	27	96	67	76	33
Th	11	6	14	7	14	10

Based on the LREE patterns (Figure 22), BRTe is the least differentiated, but Eu/Eu* for this tuff is similar to the others. Its pattern stands slightly apart from BRTn

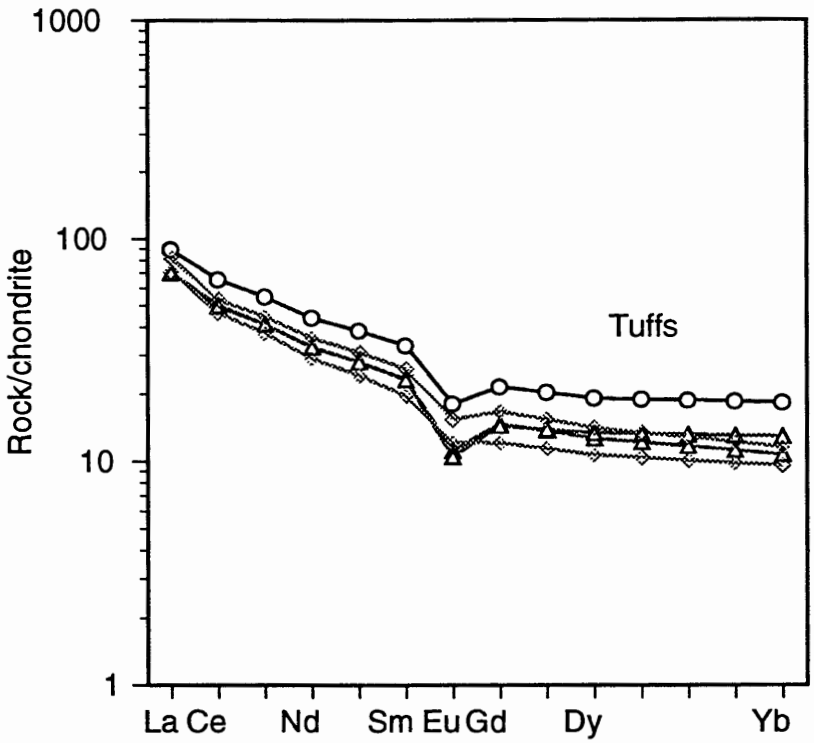

Figure 22. REE spider plot for the tuff samples. BRTn shown as open circles, BRTe as open triangles, and CPT as open diamonds. Normalization values after Nakamura (1974).

and CPT, but still falls within the range defined by the granitic rocks. CPT has the most variation in its REE values and has the lowest Eu/Eu*, which suggests that it was derived from the least differentiated magma. Most importantly, the patterns defined by the tuffs mimic those of the pluton (compare Figures 13 and 22), which provides support that the tuffs and the pluton share a cogenetic relationship.

PETROLOGIC RELATIONSHIP

The Cash Prairie tuff, Bumping River tuff-north, and the Bumping River tuff-east contain quartz and plagioclase phenocrysts, although in slightly varying abundances and sizes. This implies that, when erupted, the magma in the part of the chamber that was

tapped contained phenocrysts of quartz and plagioclase in a molten matrix. It is difficult to tie this observation directly with the plutonic samples because the pluton represent the end product of a chemically and physically dynamic system. However, it is important to note that the granitic samples also contain phenocrysts of quartz and plagioclase only. Although this relationship is far from a convincing argument to support a cogenetic relationship between the tuffs and the pluton, it is important nonetheless because it is not inconsistent with this interpretation.

IMPLICATIONS

Field, chemical, and petrographic relationships between the Mount Aix derived tuffs and the Bumping Lake pluton indicate that the pluton is the chilled remains of the magma chamber genetically related to the caldera. Establishing this genetic link between eruptive products and source is as rare as it is significant. Typically, researchers must rely on eruptive products alone as a means to model magma chamber processes because the magma chamber is not exposed. Hildreth (1979) states that, "Much of the magmatic record may either be obliterated or rendered ambiguous in granitic rocks themselves." With this statement in mind, the significance of the Bumping Lake pluton with the signature of *two* eruptions preserved at the surface becomes clear. Based on dates of BRTn and CPT, the magma chamber must have been active at least three million years during the period 28 to 25 Ma. Clasts of BRTn occur in CPT and BRTn has an older date, so the eruption that produced BRTn must have preceded that of CPT.

It is significant that a chemical match of the older BRTn can be found in the pluton even though the chamber erupted at least once more to produce the CPT. Therefore, the processes occurring in the pluton after eruption of BRTn were not sufficiently vigorous to homogenize the melt, which eliminates the possibility of vigorous convection. Instead, the chamber was disturbed only enough to mingle the chemistry of the BRTn-type magma with a subsequent magma (the difference between mingling and mixing may be thought of in terms of the difference between marbling cake batter and putting a blender in it). This independent line of reasoning concurs with the main conclusion of the section on rheology: convection could not have been turbulent but, if present, was more likely weak.

The vent for the BRTn eruption is located near Bismarck Peak (Hammond and Cole, 1992), so one might hope that the BRTn-type granite is located in the pluton near the vent. However, the BRTn-type granite samples are scattered throughout the pluton (Figure 23). With the exception of one sample, CPT-type samples cluster in the eastern part of the pluton on Nelson Ridge. The BRTn-type samples are scattered as a result of activity prior to the eruption of CPT, and to an extent, the eruption of CPT itself. Because the BRTn-type samples are found interspersed with samples that have no known extrusive equivalent, the BRTn-type magma probably mingled with one or more later batches of magma before the eruption of CPT. Also, because the distribution of CPT-type plutonic samples is confined to the southern part of the pluton, little to no convective or eruptive activity followed the eruption of CPT. Instead, the pluton probably crystallized without interruption.

Evidence that significant crystallization did not occur between the eruption of BRTn and CPT is: i) the BRTn-type granite is texturally and modally identical to the CPT-type samples; ii) BRTn-type granite is widely scattered throughout the pluton; iii) smooth chemical gradients exist in the pluton between BRTn-type granite and CPT-type granite. Internal diffusion, a process that requires a liquid phase for a high diffusion coefficient (Hanson, 1978; Hildreth, 1981), may be responsible for these smooth gradients.

The tuff that doesn't match any samples in the pluton, BRTe, has much more Zr relative to SiO_2 than BRTn and CPT. The chemistry of BRTe indicates that it is much less differentiated than the other tuffs. Therefore, BRTe probably erupted before both BRTn and CPT. Age dates indicate that BRTe erupted after BRTn, but before CPT. If

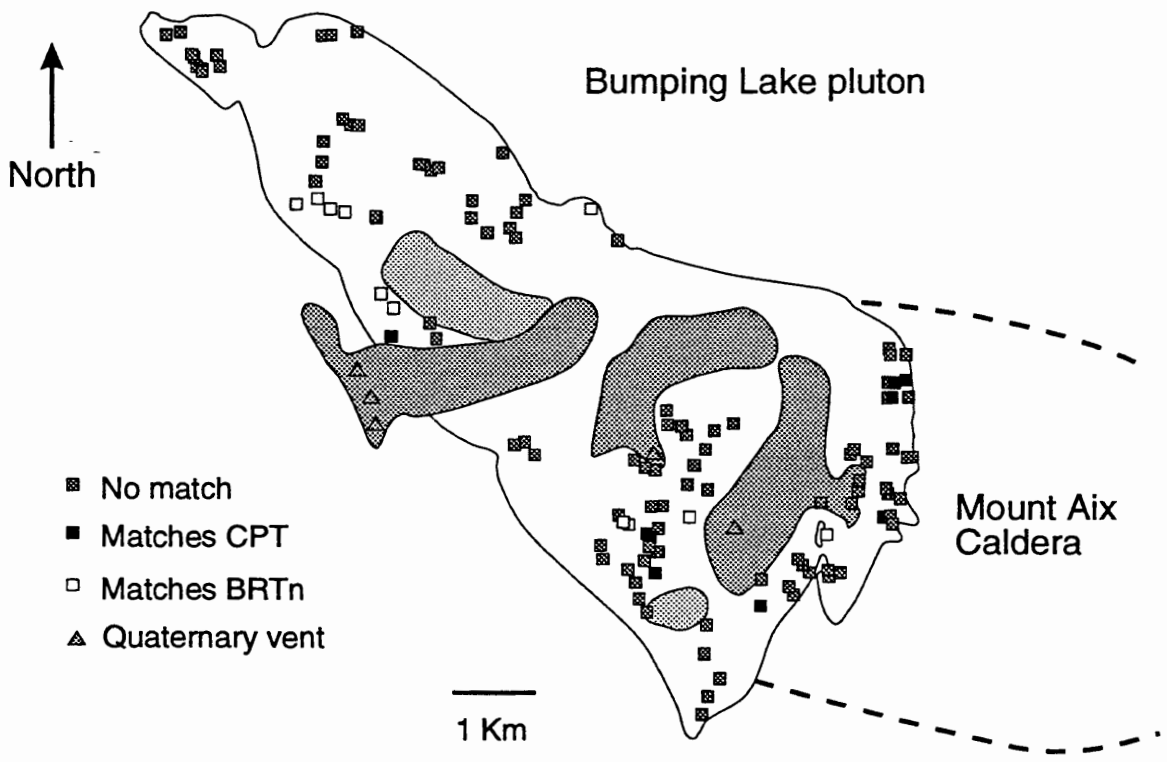

Figure 23 Location of granite samples that chemically match tuffs from the Mount Aix caldera.

these dates are accurate, then one must explain why the chemistry of both the BRTn and CPT were clearly preserved in the pluton, while the chemistry of BRTe was not. Assuming the dates are accurate, I propose that the chemistry of BRTe is preserved either beneath the caldera fill that covers the pluton in the southeast or at a deeper level in the pluton to the northwest of the caldera. In order to solve the apparent discrepancy between the chemistry and age date, a new date of BRTe should be obtained.

The vent that produced the older BRTn is preserved near Bismarck Peak. This vent is characterized by breccia margins and vertical flow structures shown by clast alignments (Paul E. Hammond, pers. commun., 1994). A sample taken from the region of vertical flow structures chemically matches the BRTn statistical population with a confidence interval of 67%. The CPT is younger than the BRTn, and since the BRTn vent is preserved, one would hope that the CPT vent would also be preserved. No other vents have been identified within the caldera margin east of the pluton. However, the caldera margin extends westward over the pluton, and the CPT may have vented in this area. Because all but one CPT-type granite samples are found in the eastern part of the pluton on Nelson ridge, the eruption that produced the CPT probably vented in this area. If this is the case, then the extrusive expression of this vent has been destroyed by erosion and by a younger intrusion of porphyritic andesite.

A possible eruptive history of the Bumping Lake pluton and Mount Aix caldera is as follows. At some point during its differentiation history, the granitic intrusion vented to the surface (possibly driven by injection of hot basalt at depth), which produced the BRTn (Figure 24a). The magma at that point was the BRTn-type magma, and had a

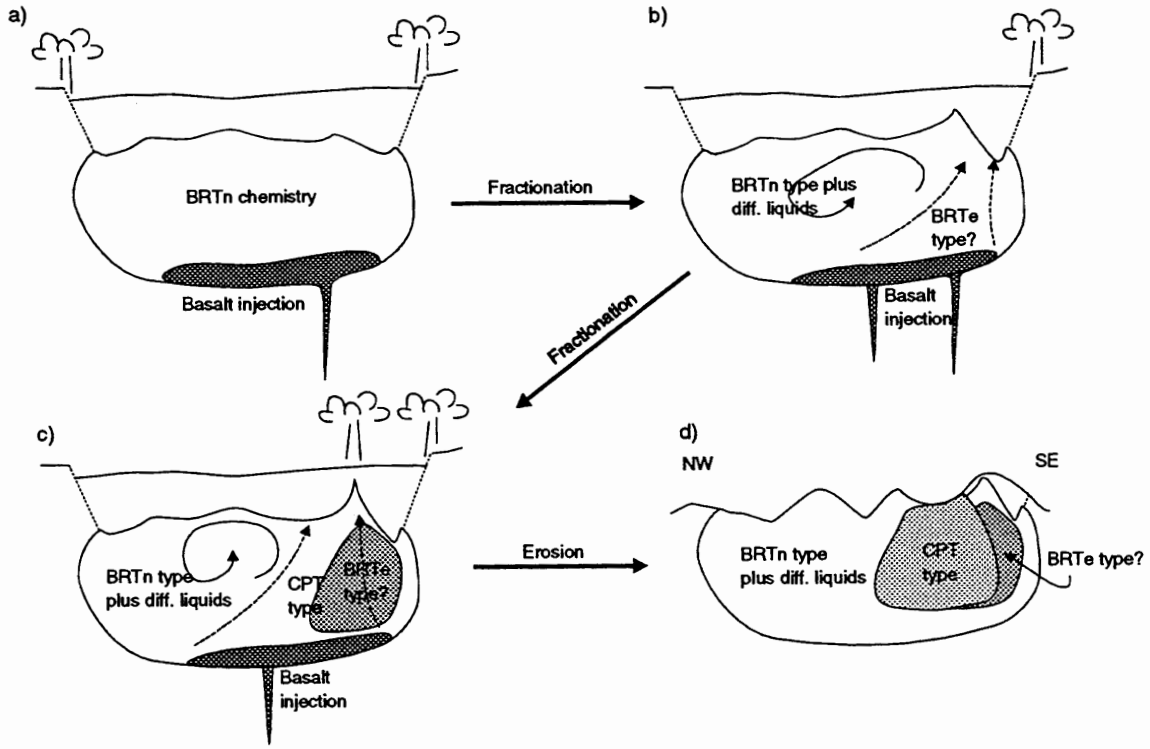

Figure 24 Schematic evolution of the pluton and caldera. The shaded regions are meant to represent regions dominated by BRTe-type magma, and CPT-type magma rather than regions composed entirely of that magma type. See text for discussion.

chemical signature identical to BRTn. Over time, fractionation continued, but the BRTn-type magma was preserved in the intrusion. A second eruption produced the BRTe. This eruption may have been localized in the southeastern region of the caldera. The chamber to the northwest was probably physically disturbed by the event causing the BRTn-type magma to mingle with more fractionated magma (Figure 24b). This process was repeated with the eruption of the CPT (Figure 24c). After eruption of CPT, the intrusion crystallized and erosion exposed the complex approximately to the extent shown in Figure 24d.

FURTHER WORK

Because of the size of the pluton and the complexity of its relationship to surrounding rocks, this study was not able to cope with every aspect of the pluton. Listed below are several of the most imporant and interesting of the questions this study raised.

1) Complete isotope work on flows from vents that cut through the Bumping Lake pluton to determine if BLP extends vertically with depth or if the pluton is tabular. If the plutons extends vertically, what is the contribution of the pluton to the chemical signature of the flows in terms of contamination and assimilation? If the pluton is tabular, then the additional information about the shape of the pluton could be used in convection models.

2) Complete isotope work on the pluton to determine source material and to verify crustal contamination.

3) Study in detail the relationship between the stoped xenoliths near the intrusive contacts, the pluton, and the host rock. Exploring the effect of assimilation on the chemistry of the pluton, and the effect of assimilating xenoliths into the pluton would be a meaningful contribution to understanding magma chamber processes.

4) Fluid inclusion work could be done on quartz phenocrysts in the tuffs and quartz from the chemically matching granite to support the link between source rock and eruptive product.

CONCLUSIONS

The source of the Bumping Lake pluton is a heterogeneous region of metasedimentary and metavolcanic rocks. Room was probably made in the shallow crust by a transtensional stress regime. Stoping of the host rock occurred in the upper level of the pluton, but its contribution to making room for the pluton was probably minimal. On a small scale, the location of the pluton may have been influenced by an anticline in the host rock and pre-existing structures in the Rimrock Lake inlier.

Granodiorite and quartz diorite formed only at the intrusive contact as a result of assimilation of the host rock. During emplacement, the magma vented at least three times, possibly as a result of injections of fresh, volatile-rich basalt at the base of the chamber. During these tuff-producing eruptions, differentiation processes such as plagioclase and accessory mineral fractionation were constantly acting. The first eruption produced the BRTe: a highly siliceous, relatively undifferentiated tuff. After an unknown period of time, a second eruption produced the highly siliceous, highly fractionated BRTn from a vent near Bismarck Peak. A three million year eruptive hiatus followed, during which the magma may have weakly convected, but not thoroughly mixed. The hiatus was broken by an eruption of the CPT, which is the least siliceous tuff, and is less fractionated than BRTn. The final eruption disrupted the magma chamber so that the BRTn-type magma mingled, but not mixed, with the CPT-type magma.

Crystallization ensued and preserved this intermingled structure. During the crystallization process, an extremely fractionated, mafic poor granite filled extensional cooling fractures where the pluton was brittle, and mingled with the pluton where still ductile. Further cooling completely crystallized the pluton.

REFERENCES

Abbott, A. T., 1953, The geology of the northwest portion of the Mt. Aix quadrangle, Washington: University of Washington Doctor of Philosophy, 256 p.

Armstrong, R. L., Harakal, J. E., and Hollister, V. F., 1976, Age determination of late Cenozoic porphyry copper deposits of the North American Cordillera: Institution of Mining and Metallurgy, v. 85, p. B239-B244.

Atwater, T., 1970, Implications of plate tectonics for the Cenozoic evolution of western North America: Geological Society of America Bulletin, v. 81, p. 3513-3536.

Bacon, C. R., and Druitt, T. H., 1988, Compositional evolution of the zoned calcalkaline magma chamber of Mount Mazama, Crater Lake, Oregon: Contributions to Mineralogy and Petrology, v. 98, p. 224-256.

Bates, R. L., and Jackson, J. A. (eds.), 1986, Dictionary of Geological Terms, 3rd edition: Doubleday, New York, 571 p.

Best, M.G., 1982, Igneous and Metamorphic Petrology: W. H. Freeman and Company, New York, 630p.

Boden, D. R., 1989, Evidence for step-function zoning of magma and eruptive dynamics, Toquima caldera complex, Nevada, Journal of Volcanology and Geothermal Research, v. 37, p. 39-57.

Brunstad, K. A., and Hammond, P. E., 1992, Caldera fill deposits, Fifes Peaks stratovolcano-caldera, east-central Cascade Range, Washington: Geological Society of America, Abstracts With Programs, v. 24, p. 11.

Campbell, N. P., 1987, Structural geology along the northwestern Columbia River basalt margin, Washington: Part II, Swauk Pass to Darland Mountain: Rockwell Hanford Operations, RHO-BWI-SA-325.

Chappell, B. W., and White, A. J. R., 1974, Two contrasting granite types: Pacific Geology, v. 8, p. 173-174.

Chappell, B. W., and White, A. J. R., 1992, I- and S-type granites in the Lachlan Fold Belt, In: The Second Hutton Symposium on the Origin of Granites and Related Rocks (P. E. Brown and B. W. Chappell, eds.): Geological Society of America Special Paper 272, p. 1-26.

Chayes, F., 1960, On correlation between variables of constant sum: Journal of Geophysical Research, v. 65, p. 4185-4193.

Chen, C. F., and Turner, J. S., 1980, Crystallization in a double-diffusive system: Journal of Geophysical Research, v. 85, p. 2573-2593.

Clarke, D. B., 1992, Granitoid rocks, Topics In Earth Sciences 7: Chapman and Hall, New York, 283 p..

Clayton, G. A., 1983, Geology of the White Pass area, south-central Cascade Range, Washington: University of Washington Master of Science thesis, 212 p.

Duncan, R. A., and Kulm, L. D., 1989, Plate tectonic evolution of the Cascades arc-subduction complex, *In*: The Eastern Pacific Ocean and Hawaii (Winterer, E. L., and Decker, R. W., eds.): Geological Society of America, Geology of North America, p. 413-438.

Erikson, E. R., Jr., 1969, Petrology of the composite Snoqualmie batholith, central Cascade Mountains, Washington: Geological Society of America Bulletin, v. 80, p. 2213-2236.

Evarts, R. P., Ashley, R. P., and Smith, J. G., 1987, Geology of the Mount Saint Helens area: record of discontinuous volcanic and plutonic activity in the Cascade arc of southern Washington: Journal of Geophysical Research, v. 93, p. 10,155-10,169.

Fiske, R. S., Hopson, C. A., and Waters, A. C., 1963, Geology of Mount Rainier National Park, Washington: United States Geological Survey Professional Paper 444, 93 p.

Fourcade, S., and Allegre, C. J., 1981, Trace elements behavior in granite genesis: A case study - The calcalkaline plutonic association from the Querigut Complex (Pyrenees, France): Contributions to Mineralogy and Petrology, v. 76, p. 177-195.

Fridrich, C. J., and Mahood, G. A., 1987, Compositional layers in the zoned magma chamber of the Grizzly Peak Tuff: Geology, v. 15, p. 299-303.

Halliday, A. N., Stephens, W. E., and Harmon, R. S., 1981, Isotopic and chemical constrains on the development of peraluminous Caledonian and Acadian granites: Canadian Mineralogist, v. 19, p. 205-216.

Hammond, P. E., 1989, Guide to Geology of the Cascade Range, 28th International Geological Congress, Field Trip Guidebook T306: Americal Geophysical Union, Washington, D. C., 215 p.

Hammond, P. E., and Hooper, P. R., 1991, Fifes Peaks Formation, Washington Cascade Range: 14th Annual Meeting, Oregon Academy of Science, Monmouth, OR.

Hammond, P. E., and Cole, S. F., 1992, Preliminary investigation of Mount Aix caldera, Cascade Range, Washington: Eos (Transactions of the American Geophysical Union), v. 73, no. 43, p. 612.

Hammond, P. E., King, J. F., Hooper, P. R., and Cole, S. F., 1993, Mount Aix caldera-Bumping Lake pluton, Cascade Range, Washington -- Revised findings: Eos (transactions of the American Geophysical Union), v. 74, no. 43, p. 643-644.

Hanson, G. N., 1978, The application of trace elements to the petrogenesis of igneous rocks of granitic composition: Earth and Planetary Science Letters, v. 38, p. 26-43.

Hartman, D. A., 1973, Geology and low-grade metamorphism of the Greenwater River area, central Cascade Range, Washington: University of Washington Doctor of Philosophy thesis, 99p.

Hildreth, W., 1979, The Bishop Tuff: Evidence for the origin of compositional zonation in silicic magma chambers: Geological Society of America Special Paper 180, p. 43-75.

Hildreth, W., 1981, Gradients in silicic magma chambers: implications for lithospheric magmatism: Journal of Geophysical Research, v. 86, p. 10,153-10,192.

Hooper, P. R., Johnson, D. M., and Conrey, R. M., 1993, Major and trace element analyses of rocks and minerals by automated X-ray spectrometry: Washington State University, Geology Department, Open File Report, 36 p.

Katsui, Y., 1963, Evolution and magmatic history of some Krakatoan calderas in Hokkaido, Japan: Journal of the Faculty of Science at Hokkaido University, v. 11, p. 631-650.

Long, P. E., and Duncan, R.A., 1983, 40Ar/39Ar ages of Columbia River Basalt from deep boreholes in south-central Washington: [abstr.] Eos (American Geophysical Union Transactions), v. 64, p. 90.

Lux, D. R., 1981, Geochronology, geochemistry,and petrogenesis of basaltic rocks from the western Cascades, Oregon: Ohio State University Doctor of Philosophy thesis, 171p.

Mahood, G. A., and Cornejo, P. C., 1992, Evidence for ascent of differentiated liquids in a silicic magma chamber found in a granitic pluton, *In*: The Second Hutton Sym-

posium on the Origin of Granites and Related Rocks (P.E. Brown and B.W. Chappell, eds.): Geological Society of America Special Paper 272, p. 63-70.

Marsh, B. D., 1989, On convective style and vigor in sheet-like magma chambers: Journal of Petrology, v. 30, p. 479-530.

McBirney, and A. R., Murase, T., 1984, Rheological properties of magmas: Annual Review of Earth and Planetary Sciences, v. 12, p. 337-357.

Miller, C. F., and Mittlefehldt, D. W., 1982, Depletion of light rare-earth elements in felsic magmas: Geology, v. 10, p. 129-133.

Miller, C. F., Watson, E. B., and Harrison, T. M., 1987, Perspectives on the source, segregation, and transport of granitoid magmas: Royal Society of Edinburgh Earth Sciences Transactions, v. 79, p. 135-156.

Miller, R. B., 1985, The pre-Tertiary Rimrock Lake inlier, southern Cascades, Washington: Washington Division of Geology and Earth Resources Open File Report 85-2, 20 p.

Murphy, M. T., and Marsh, B. D., 1993, Textures and magmatic evolution of intermediate-composition dome complexes: Evidence from the northern Tatoosh complex, southern Washington Cascades: Journal of Volcanology and Geothermal Research, v. 54, p. 197-220.

Nakamura, N., 1974, Determination of REE, Ba, Fe, Mg, Na, and K in carbonaceous and ordinary chondrites: Geochimica et Cosmochimica Acta, v. 38, p. 757-773.

Nilson, R.H., McBirney, A.R., and Baker, B.H., 1985, Liquid fractionation. Part II: Fluid dynamics and quantitative implications for magmatic systems: Journal of Volcanology and Geothermal Research, v. 24, p. 25-54.

Norman, M. D., Leeman, W. P., and Mertzman, S. A., 1992, Granites and rhyolites from the northwestern USA: temporal variation in magmatic processes and relations to tectonic setting, In: The Second Hutton Symposium on the Origin of Granites and Related Rocks (P.E. Brown and B.W. Chappell, eds.): Geological Society of America Special Paper 272, p. 71-82.

Pankhurst, R. J., 1979, Isotope and trace element evidence for the origin and evolution of Caledonian granites in the Scottish Highlands, In: Origin of Granite Batholiths: Geochemical Evidence (M.P. Atherton and J. Tarney, eds.), p. 18-33.

Pearce, J. A., Harris, N. B. W., and Tindle, A. G., 1984, Trace element discrimination diagrams for the tectonic interpretation of granitic rocks: Journal of Petrology, v. 25, p. 956-983.

Petford, N., Kerr, R. C., and Lister, J. R., 1993, Dike transport of granitoid magmas: Geology, v. 21, p. 845-848.

Riddihough, R., 1984, Recent movements of the Juan de Fuca plate system: Journal of Geophysical Research, v. 89, p. 6980-6994.

Schasse, H. W., 1987, Geologic Map of the Mount Rainier quadrangle, Washington: Washington Division of Geology and Earth Resources Open File Report 87-16, 43 p.

Schreiber, S. A., 1981, Geology of the Nelson Butte area, south-central Cascade Range, Washington: University of Washington Master of Science thesis, 81 p.

Seager, W. R., and McCurry, M., 1988, The cogenetic Organ cauldron and batholith, south-central New Mexico: Evolution of a large-volume ash-flow cauldron and its source magma: Journal of Geophysical Research, v. 93, p. 4421-4433.

Simmons, G. C., Van Noy, R. M., and Zilka, N. T., 1974, Mineral resources of the Cougar Lake study area: United States Geological Survey Open File Report, p. 74-243.

Smith, R. L., and Bailey, R. A., 1966, The Bandelier tuff: a study of ash-flow eruption cycles from zoned magma chambers: Bulletin of Volcanology, v. 29, p. 83-104.

Smith, R. L., 1979, Ash-flow magmatism: Geological Society of America Special Paper 180, p.5-27

Sparks, R. S. J., Huppert, H. E., and Turner, J. S., 1985, The fluid dynamics of evolving magma chambers: Philosophical Transactions of the Royal Society of London, v. A310, p. 511-534.

Spera, F. J., 1980, Thermal evolution of plutons: a parameterized approach: Science, v. 207, p. 299-301.

Spera, F. J., Yuen, D. A., and Kirschvink, S. J., 1982, Thermal boundary layer convection in silicic magma chambers: effects of temperature-dependent rheology and implications for thermogravitational chemical fractionation: Journal of Geophysical Research, v. 87, p. 8755-8767

Spera, F. J., Yuen, D. A., Greer, J. C., and Sewell, G., 1986, Dynamics of magma withdrawal from stratified magma chambers: Geology, v. 14, p. 723-726.

Stephens, W. E., and Halliday, A. N., 1979, Compositional variation in the Galloway plutons, In: Origin of Granite Batholiths: Geochemical Evidence (M.P. Atherton and J. Tarney, eds.), p. 9-17.

Stephens, W. E., 1992, Spacial, compositional, and rheological constraints on the origin of zoning in the Criffell Pluton, Scotland, In: The Second Hutton Symposium on the Origin of Granites and Related Rocks (P.E. Brown and B.W. Chappell, eds.): Geological Society of America Special Paper 272, p. 191-200.

Swanson, D. A., 1966, Tieton volcano, a Miocene eruptive center in the southern Cascade Mountains, Washington: Geological Society of America Bulletin, v. 77, p. 1293-1314.

Swanson, D. A., 1978, Geologic map of the Tieton River area, Yakima County, south-central Washington, scale 1:48,000: United States Geological Survey Miscellaneous Field Studies, Map MF-968.

Tabor, R. W., Engels, J. C., and Staatz, M. H., 1968, Quartz diorite-quartz monzonite and granite plutons of the Pasayten River area, Washington: petrology, age and emplacement: United States Geological Survey Professional Paper 600-C, p. 45-52.

Turner, J. S., and Gustafson, L. B., 1981, Fluid motions and compositional gradients produced by crystallization or melting at vertical boundaries: Journal of Volcanology and Geothermal Research, v. 11, p. 299-318.

Turner, J. S., and Campbell, I. H., 1986, Convection and mixing in magma chambers: Earth Science Review, v. 23, p. 245-252.

Vance, J. A., Clayton, G. A., Mattinson, J. M., and Naeser, C. W., 1987, Early and middle Cenozoic stratigraphy of the Mount Rainier-Tieton River area, southern Washington Cascades: Washington Division of Geology and Earth Resources Bulletin, v. 77, p. 269-290.

Walsh, T. J., Korosec, M. A., Phillips, W. M., Logan, R. L., and Schasse, H. W., 1987, Geologic map of Washington - southwest quadrant, scale 1:250,000: Washington Division of Geology and Earth Resources, Geologic Map GM-34.

Watkins, N. D., and Baksi, A. K., 1974, Magnetostratigraphy and oroclinal folding of the Columbia River, Steens, and Owyhee Basalts in Oregon, Washington, and Idaho: American Journal of Science, v. 274, p. 148-189.

Whitney, J. A., Dorais, M. J., Stormer, J. C. Jr., Kline, S. W., and Matty, D. J., 1988, Magmatic conditions and development of chemical zonation in the Carpenter Ridge tuff, central San Juan volcanic field, Colorado: American Journal of Science, v. 63, p. 324-329.

Williams, H., 1942, The geology of Crater Lake National Park, Oregon, with a reconnaissance of the Cascade Range southwards to Mount Shasta: Carnegie Institute of Washington Publications, v. 540, 162 p.

Winters, W. J., 1984, Stratigraphy and sedimentology of Paleogene arkosic and volcaniclastic strata, Johnson Creek-Chambers Creek area, southern Cascade Range, Washington: Portland State University Master of Science thesis, 162 p.

APPENDIX A

ANALYTICAL METHODS

A total of 154 samples were collected for this study, 138 of which were chemically analyzed and 12 representative samples were studied petrographically. The samples were chipped at Portland State University, and then sieved using a plastic 0.25 inch mesh. The chips were sorted and only those chips with no weathered surfaces were kept. Samples were brought to Washington State University's GeoAnalytical Laboratory in Pullman, Washington and prepared for X-ray fluorescence (XRF) and inductively coupled plasma - mass spectrometry (ICP-MS) according to the procedure outlined by Hooper and others, 1993, and then analyzed. Because tungsten carbide crushing bowls were used, samples were contaminated with tungsten, cobalt, tantalum, and less than two ppm niobium. Tungsten, cobalt, and tantalum are not analyzed by XRF so contamination of these elements can be ignored. Niobium concentrations may be used because instrumental precision of XRF is not high enough to detect the contamination. However, due to the high precision of the ICP-MS method, niobium and tantalum contamination can be detected, and these elements are therefore ignored.

APPENDIX B

XRF RESULTS

Area	Copper Creek	American Ridge	American Ridge	Miner's Ridge	American Ridge	Miner's Ridge	Miner's Ridge
Desc.	aphanite	fine granite	fine granite	fine granite	fine granite	fine granite	fine granite
Chem #	162	285	194	256	195	254	261
UTM East	629327	619679	622103	624945	621752	624933	625679
UTM North	5185604	5191800	5190988	5185170	5190409	5184406	5185945
SiO2	77.54	76.01	76.99	77.24	77.51	77.64	77.97
Al2O3	12.28	12.83	12.74	12.84	12.99	12.29	12.62
TiO2	0.059	0.157	0.125	0.105	0.095	0.070	0.088
FeO*	0.82	1.24	1.07	0.72	0.47	0.78	0.53
MnO	0.011	0.023	0.018	0.014	0.007	0.011	0.020
CaO	0.52	1.00	0.61	0.71	0.47	0.57	0.86
MgO	0.00	0.14	0.42	0.10	0.29	0.00	0.03
K2O	5.40	4.88	5.05	5.21	5.27	5.57	4.37
Na2O	3.36	3.69	2.97	3.05	2.89	3.06	3.51
P2O5	0.006	0.027	0.021	0.012	0.012	0.007	0.010
Ni	11	7	9	8	9	8	12
Cr	0	2	0	0	0	0	0
Sc	10	4	8	5	2	4	3
V	0	13	0	0	0	0	0
Ba	67	329	543	692	326	452	490
Rb	184	147	139	159	153	140	130
Sr	9	82	57	53	59	34	78
Zr	112	122	115	103	102	87	103
Y	36	15	37	30	29	16	33
Nb	13.2	10.5	11.6	15.5	16.7	6.5	14.4
Ga	17	12	14	15	14	11	10
Cu	41	15	9	17	16	31	9
Zn	19	21	17	14	11	20	8
Pb	12	11	9	9	8	14	7
La	35	25	35	17	24	26	33
Ce	67	51	42	56	47	52	51
Th	35	32	30	29	22	24	30

Area	Miner's Ridge	American Ridge	Granite Lake	Pear Butte Ridge	Miner's Ridge	Pear Butte Ridge	Pear Butte Ridge
Desc.	fine granite	fine granite	granite	granite	granite	granite	granite
Chem #	258	274	10	164	183	234	167
UTM East	625261	621867	626110	628903	624824	627945	628370
UTM North	5186479	5190800	5184817	5182896	5183707	5182618	5183037
SiO2	77.98	78.13	70.00	70.01	70.37	70.42	70.60
Al2O3	12.62	12.60	15.45	15.12	14.85	15.51	15.72
TiO2	0.078	0.064	0.420	0.321	0.317	0.419	0.396
FeO*	0.48	0.46	3.10	3.36	2.92	3.46	2.66
MnO	0.008	0.006	0.040	0.043	0.045	0.036	0.038
CaO	0.55	0.36	3.03	3.42	2.57	2.72	2.97
MgO	0.00	0.00	0.72	0.50	1.11	0.63	0.74
K2O	4.89	5.10	2.47	2.72	3.05	2.51	2.35
Na2O	3.38	3.27	4.65	4.43	4.70	4.18	4.42
P2O5	0.008	0.004	0.110	0.084	0.077	0.106	0.099
Ni	10	11	7	6	6	7	5
Cr	0	4	7	6	4	6	4
Sc	6	5	7	8	9	13	11
V	8	0	35	13	22	30	24
Ba	320	79	661	895	769	749	701
Rb	151	205	70	67	105	83	82
Sr	56	17	213	204	167	231	228
Zr	94	102	179	167	159	183	172
Y	20	24	21	20	27	14	14
Nb	21.0	8.7	10.3	9.1	10.1	10.2	6.8
Ga	12	12	19	15	19	15	17
Cu	10	14	32	206	42	106	119
Zn	6	26	46	45	33	40	61
Pb	8	8	7	15	7	8	13
La	35	12	40	49	13	24	28
Ce	81	29	45	82	49	44	43
Th	42	23	11	12	9	9	10

APPENDIX B

XRF RESULTS

Miner's Ridge granite	American Ridge granite	Pear Butte Ridge granite	Nelson Ridge granite	Deep Creek granite	Miner's Ridge granite	Pear Butte Ridge granite	American Ridge granite
173	284	169	154	170	245	166	188
626012	619806	627279	630109	626370	624855	628200	619127
5181896	5191764	5182177	5186787	5180677	5183164	5183177	5188122
70.62	70.63	70.71	71.00	71.28	71.34	71.36	71.36
15.10	14.76	14.87	15.03	14.59	15.09	15.25	15.09
0.372	0.391	0.414	0.344	0.320	0.302	0.362	0.281
3.20	3.09	3.37	3.03	3.51	2.56	2.76	2.53
0.070	0.056	0.056	0.040	0.059	0.047	0.038	0.047
2.61	2.21	2.74	2.61	2.28	2.49	2.79	2.01
1.03	0.57	0.60	0.45	0.58	0.44	0.59	0.97
2.50	3.49	2.92	3.00	3.19	3.00	2.72	3.75
4.41	4.70	4.22	4.41	4.12	4.65	4.05	3.90
0.092	0.099	0.101	0.082	0.077	0.069	0.090	0.059
6	8	6	6	6	7	3	4
5	0	2	3	6	6	2	0
13	7	13	7	11	6	10	11
19	37	19	21	17	20	24	14
750	799	709	702	726	723	947	687
80	98	103	109	106	91	79	132
183	182	175	167	153	168	226	140
172	207	168	189	187	182	162	165
26	22	22	29	25	28	13	24
9.3	12.2	10.2	11.4	9.3	12.1	8.8	10.9
17	17	18	21	19	16	16	18
13	28	55	126	7	36	57	36
44	39	47	46	71	38	40	27
13	13	13	9	23	10	8	7
25	54	31	19	30	17	34	35
67	71	57	63	62	50	24	78
11	19	12	13	11	13	8	15

Nelson Ridge granite	Miner's Ridge granite	Nelson Ridge granite	Pear Butte Ridge granite	Miner's Ridge granite	Miner's Ridge granite	Miner's Ridge granite	Miner's Ridge granite
5	174	219	165	246	249	175	215
630143	624533	630333	628667	624758	624994	624624	625667
5184682	5182683	5187140	5183768	5182024	5183897	5182354	5184890
71.42	71.47	71.61	71.64	71.66	71.67	71.73	71.74
14.95	14.86	15.08	14.99	14.97	15.41	14.74	15.33
0.380	0.314	0.331	0.321	0.307	0.382	0.313	0.285
2.70	3.19	2.72	2.77	2.64	3.01	3.02	1.84
0.030	0.043	0.042	0.039	0.050	0.050	0.040	0.031
3.10	1.84	2.58	2.76	1.98	2.05	1.82	2.90
0.74	0.83	0.44	0.46	0.40	0.39	0.88	0.45
2.64	3.23	2.66	2.98	3.52	2.71	3.12	3.36
3.95	4.15	4.44	3.95	4.40	4.25	4.28	4.00
0.090	0.072	0.080	0.075	0.071	0.091	0.066	0.061
6	7	9	5	7	9	8	5
5	5	5	5	1	4	4	6
8	12	9	5	7	4	10	6
36	19	23	24	13	31	13	43
820	849	731	714	838	756	794	1064
81	114	90	66	135	70	109	95
227	159	178	210	157	175	183	244
172	185	180	139	183	190	177	150
13	27	25	8	27	22	25	5
7.3	12.1	14.2	5.7	11.6	11.5	9.3	3.6
15	18	15	14	20	21	18	16
109	10	50	32	96	112	19	21
26	40	36	42	45	36	29	31
7	15	7	5	13	11	5	8
40	18	37	20	27	27	35	9
46	53	51	40	58	45	62	12
11	10	14	8	13	12	12	11

APPENDIX B

XRF RESULTS

Nelson Ridge granite	Nelson Ridge granite	Miner's Ridge granite	Nelson Ridge granite	Miner's Ridge granite	Nelson Ridge granite	Nelson Ridge granite	Deep Creek granite
220	153	241	148	247	149	160	172
630588	630321	624909	630145	624994	630309	630079	626182
5187104	5186811	5183661	5187750	5182933	5187683	5184165	5180244
71.90	71.99	72.08	72.08	72.16	72.20	72.21	72.30
14.77	14.84	14.65	14.41	14.86	14.68	14.80	14.37
0.294	0.277	0.301	0.301	0.286	0.314	0.282	0.300
2.72	2.53	2.77	2.92	2.91	2.87	2.69	3.00
0.039	0.040	0.042	0.054	0.039	0.037	0.028	0.050
2.35	2.27	2.14	2.25	1.51	2.03	2.54	2.00
0.39	0.45	0.39	0.38	0.38	0.37	0.38	0.36
3.03	3.02	3.34	3.19	3.04	3.15	2.94	3.24
4.43	4.52	4.22	4.34	4.75	4.27	4.06	4.30
0.068	0.063	0.081	0.069	0.066	0.071	0.074	0.068
9	6	10	6	11	5	6	7
4	0	3	5	3	3	2	4
9	6	8	8	6	9	7	13
13	0	15	18	11	16	18	9
733	777	900	719	920	791	824	740
101	104	104	111	119	134	75	101
158	161	152	145	172	152	185	143
181	178	179	186	180	185	169	191
30	29	29	30	31	31	26	31
12.9	10.5	12.3	11.1	12.8	11.6	10.9	13.0
17	17	17	18	18	16	17	16
82	40	30	22	33	167	65	15
39	45	42	30	30	32	36	37
9	12	7	5	6	7	9	10
18	33	28	30	21	24	42	28
54	58	55	65	53	52	60	78
12	9	13	13	12	11	11	12

Pear Butte Ridge granite	Miner's Ridge granite	Nelson Ridge granite	Hwy 410 granite	Miner's Ridge granite	American Ridge granite	Hwy 410 granite	Miner's Ridge granite
233	243	217	213	186	192	290	263
628030	624970	630194	618279	626673	624152	618152	626273
5182424	5183364	5187689	5194750	5186171	5190134	5194770	5186055
72.30	72.35	72.42	72.68	72.78	72.94	73.14	73.23
15.02	15.14	14.50	14.69	14.51	15.02	14.34	14.83
0.339	0.339	0.303	0.244	0.256	0.192	0.241	0.217
2.62	2.67	2.71	2.37	1.55	1.83	2.23	1.67
0.033	0.044	0.050	0.032	0.023	0.031	0.036	0.019
2.21	1.94	2.26	2.11	2.32	1.81	2.00	2.37
0.48	0.45	0.35	0.61	0.87	0.74	0.30	0.27
2.87	2.26	2.94	3.24	3.25	3.37	3.39	3.47
4.04	4.73	4.40	3.98	4.37	4.03	4.26	3.89
0.093	0.081	0.070	0.052	0.059	0.046	0.053	0.046
9	11	10	5	5	6	14	9
9	7	3	1	3	4	12	1
11	6	9	7	11	10	8	5
31	20	14	11	10	0	13	5
849	728	791	779	1065	839	854	1005
86	76	110	115	100	101	134	99
190	190	157	152	220	158	150	185
149	191	190	157	148	132	141	138
14	27	28	19	8	15	27	15
9.3	12.2	14.8	8.5	4.6	7.7	10.8	8.7
16	19	16	15	17	17	16	17
49	14	52	14	10	7	7	32
40	51	40	23	17	28	21	15
9	17	9	8	6	9	7	8
33	42	25	23	44	20	36	22
46	42	48	58	53	48	53	44
13	12	10	16	14	16	17	14

APPENDIX B

XRF RESULTS

American Ridge granite	Miner's Ridge granite	American Ridge granite	Miner's Ridge granite	Copper Creek granite	American Ridge granite	American Ridge granite
269	253	189	178	163	190	283
620091	624873	619079	623818	629630	620139	619927
5188067	5183552	5188671	5183323	5185488	5188073	5191752
73.28	73.35	73.36	73.46	73.55	73.59	73.72
14.12	14.43	14.28	14.32	14.47	14.29	13.85
0.244	0.233	0.247	0.207	0.263	0.220	0.247
2.24	1.87	2.03	1.90	1.70	1.79	2.04
0.042	0.039	0.031	0.031	0.022	0.036	0.038
1.83	1.80	1.97	1.83	2.17	1.90	1.78
0.38	0.18	0.74	0.79	0.45	0.76	0.38
3.75	3.79	3.62	3.66	3.26	3.52	3.98
4.04	4.26	3.65	3.76	4.05	3.85	3.90
0.051	0.049	0.052	0.047	0.059	0.043	0.060
9	11	7	8	8	6	9
1	4	4	2	1	1	2
5	2	10	9	11	7	4
23	22	8	3	25	9	10
866	836	826	806	824	784	823
128	129	130	129	122	122	108
136	140	140	136	158	137	151
150	141	141	119	154	123	158
19	35	30	18	20	21	16
10.8	11.8	11.2	9.2	8.8	9.1	13.2
16	17	16	14	16	15	14
9	17	46	25	19	11	37
26	47	28	23	26	21	34
6	9	9	9	9	7	11
19	131	42	13	11	33	38
20	245	89	51	33	55	57
18	30	16	18	14	20	19

Miner's Ridge granite	Hwy 410 granite	Nelson Ridge granite	American Ridge granite	Miner's Ridge granite	Rainier Fk. Ridge granite	Rainier Fk Ridge granite
259	210	158	201	182	203	205
625303	617545	630242	618879	624436	618121	617412
5186230	5194677	5184018	5189030	5183945	5190768	5191451
73.76	73.77	73.84	73.84	73.94	73.95	73.99
14.71	13.97	13.81	14.08	14.09	13.83	13.96
0.175	0.225	0.253	0.204	0.208	0.230	0.293
1.44	2.04	2.14	1.81	1.66	1.93	1.82
0.020	0.032	0.029	0.036	0.030	0.037	0.021
2.23	1.95	1.95	1.68	1.64	1.77	2.00
0.14	0.50	0.17	0.58	0.83	0.49	0.60
3.25	3.64	3.88	4.03	4.00	3.81	3.43
4.25	3.82	3.86	3.69	3.56	3.89	3.84
0.035	0.049	0.067	0.044	0.040	0.056	0.047
8	4	7	6	7	8	7
4	3	0	3	4	0	1
3	7	3	9	3	3	6
11	18	11	7	6	0	17
870	816	1173	761	847	800	821
98	123	86	143	130	130	129
204	140	156	124	116	129	148
105	130	164	122	117	131	149
8	20	17	23	26	23	17
5.4	8.6	5.3	11.0	10.8	12.4	10.3
14	16	14	15	14	14	19
24	10	55	10	9	20	21
17	24	38	22	28	25	17
9	11	8	8	10	7	6
16	20	30	31	62	26	46
15	37	31	70	91	39	66
14	16	7	21	22	21	16

APPENDIX B

XRF RESULTS

Miners Ridge granite	Rainier Fk Ridge granite	Pear Butte Ridge granite	American Ridge granite	Hwy 410 granite	Rainier Fk Ridge granite	Copper Creek granite	Rainier Fk Ridge granite
248	204	230	197	91	287	8	289
625727	617655	628703	621236	617673	617503	629317	617594
5184145	5190860	5184485	5190262	5194667	5190982	5185571	5191897
73.74	74.04	74.12	74.13	74.15	74.17	74.27	74.28
13.81	14.28	14.69	13.44	13.54	13.94	13.69	14.02
0.291	0.211	0.250	0.282	0.211	0.222	0.240	0.247
3.08	1.66	1.07	2.01	2.08	1.99	1.98	1.58
0.034	0.021	0.020	0.040	0.036	0.017	0.020	0.025
1.66	2.06	2.18	1.47	1.78	1.74	2.11	2.05
0.33	0.73	0.27	0.68	0.36	0.24	0.27	0.27
3.09	3.46	3.25	4.57	4.28	3.92	3.54	3.52
3.92	3.48	4.10	3.30	3.52	3.71	3.84	3.96
0.052	0.047	0.050	0.064	0.042	0.045	0.050	0.049
8	6	10	6	9	8	9	9
3	7	4	0	0	5	2	2
4	6	16	6	5	6	5	9
10	8	4	20	15	18	0	17
696	808	818	1083	913	874	716	850
92	118	107	137	124	131	101	111
132	150	171	152	158	149	127	160
141	121	148	136	117	143	121	150
24	19	20	9	8	23	21	18
13.7	7.9	10.4	6.9	5.8	9.3	18.4	10.6
16	14	15	13	12	16	10	15
7	23	16	25	24	28	32	13
27	17	20	42	28	15	20	17
12	9	8	11	9	5	4	11
50	27	35	14	26	46	57	49
81	64	61	46	33	88	65	85
14	13	17	20	19	20	16	15

Miner's Ridge granite	Copper Creek granite	Miner's Ridge granite	Miner's Ridge granite	Copper Cr granite	Nelson Ridge granite	Miner's Ridge granite	Pear Butte Ridge granite
177	226	262	180	161	150	176	168
624279	629527	626036	624139	629345	630430	625030	628491
5182976	5184957	5185697	5184183	5184476	5187677	5184421	5182945
74.00	74.46	74.50	74.61	74.65	74.65	74.78	75.05
14.16	14.09	14.19	14.28	14.20	13.37	14.05	13.95
0.184	0.215	0.209	0.179	0.203	0.287	0.236	0.179
2.17	1.57	1.22	1.16	1.39	2.11	1.87	1.01
0.041	0.020	0.021	0.032	0.015	0.028	0.027	0.023
1.69	2.04	2.10	1.71	2.29	1.97	1.35	1.83
0.84	0.20	0.27	0.74	0.13	0.35	0.30	0.30
2.92	3.62	3.91	3.69	3.15	3.27	3.84	3.99
3.94	3.75	3.54	3.57	3.94	3.89	3.49	3.63
0.042	0.045	0.043	0.040	0.042	0.068	0.055	0.035
5	9	6	7	7	5	8	9
1	5	5	4	6	1	3	3
5	7	3	7	5	10	6	11
0	10	26	9	0	0	7	0
892	829	1067	799	779	1178	657	1103
81	113	108	105	98	83	107	84
115	147	204	141	169	150	110	147
153	133	132	123	122	171	142	124
27	20	8	15	16	12	18	27
10.5	8.7	4.8	9.2	8.5	6.2	9.3	6.9
17	14	11	14	15	13	15	15
73	8	9	11	33	22	18	61
39	16	16	33	23	25	20	39
6	5	7	13	5	8	7	9
29	16	26	18	59	18	16	42
43	48	32	44	92	32	46	63
11	12	14	21	16	6	12	16

APPENDIX B

XRF RESULTS

Cougar Lk Ridge granite	Miner's Ridge granite	Cougar Lk Ridge granite	Miner's Ridge granite	Miner's Ridge granite	American Ridge granite	Rainier Fk R. granite
191	251	270	179	255	281	208
622024	623897	622218	623848	624921	620855	618200
5185744	5183158	5185570	5183561	5184418	5190988	5192750
74.34	75.13	75.15	75.19	75.27	75.31	75.33
13.65	13.49	13.29	13.55	13.88	13.05	13.11
0.213	0.200	0.193	0.151	0.183	0.190	0.217
1.76	1.72	1.54	1.32	1.63	1.70	1.58
0.031	0.025	0.043	0.028	0.019	0.031	0.021
1.60	1.22	1.52	1.33	1.66	1.21	1.19
0.79	0.21	0.21	0.90	0.17	0.25	0.59
3.95	4.32	4.03	4.17	3.41	4.70	5.18
3.63	3.64	3.98	3.31	3.73	3.52	2.74
0.042	0.038	0.040	0.034	0.044	0.031	0.041
7	9	11	6	8	10	4
2	3	2	3	4	3	2
13	0	4	5	7	7	5
8	0	5	0	15	2	16
689	882	718	839	802	736	953
142	152	139	135	96	154	151
114	106	118	110	133	114	122
130	112	116	99	124	112	124
16	16	20	16	20	11	6
11.3	12.0	11.8	6.5	9.5	7.6	5.6
14	13	15	12	15	12	14
24	20	8	23	54	26	15
26	22	22	16	30	30	22
6	6	8	9	7	16	6
18	11	30	19	27	22	13
27	32	57	51	57	44	22
22	19	23	14	15	23	22

Rainier Fk Ridge granite	Miner's Ridge granite	Hwy 410 granite	American Ridge granite	Miner's Ridge granite	Cougar L. Ridge granite	Miner's Ridge granite
209	252	212	282	184	271	260
618333	624255	617673	620115	624770	621739	625448
5192707	5184091	5194671	5191733	5185561	5185721	5186127
75.06	75.45	75.93	76.18	76.24	76.26	76.30
13.25	13.85	13.59	13.22	13.06	13.05	13.03
0.288	0.207	0.115	0.161	0.134	0.150	0.151
1.78	1.00	1.09	0.76	1.10	1.23	1.21
0.027	0.050	0.021	0.018	0.016	0.017	0.017
1.48	2.02	1.54	1.41	1.02	1.23	1.05
0.32	0.16	0.20	0.16	0.36	0.07	0.08
4.23	2.90	4.10	4.55	4.78	4.54	4.60
3.58	4.34	3.38	3.51	3.27	3.43	3.54
0.050	0.028	0.024	0.033	0.027	0.025	0.024
7	9	6	10	9	10	9
2	2	4	3	4	3	1
3	0	0	9	3	8	5
12	2	0	0	12	4	2
899	622	806	787	575	660	841
114	81	108	130	143	138	149
142	161	120	107	77	99	76
122	127	86	106	105	102	109
8	18	11	21	17	12	31
6.8	9.3	6.1	10.0	11.6	5.9	10.2
15	13	13	11	14	14	15
18	23	7	56	3	30	15
20	37	18	17	16	15	19
6	10	6	11	8	7	8
5	19	0	9	32	28	104
40	30	7	25	29	43	179
16	22	10	20	23	15	27

APPENDIX B

XRF RESULTS

Pear Butte Ridge granite	American Ridge granite	American Ridge granite	Miner's Ridge granite	Hwy 410 granite	Copper Creek granite	Nelson Ridge granodiorite
231	193	280	185	211	157	159
628727	623691	620830	625861	617673	629467	630200
5183733	5190982	5190679	5185293	5194671	5184726	5184116
75.36	75.43	76.78	77.09	77.20	77.27	65.78
13.80	13.47	12.70	13.20	12.96	12.86	16.43
0.197	0.174	0.133	0.165	0.100	0.138	0.567
1.04	1.56	1.13	1.08	0.87	0.68	5.13
0.014	0.022	0.011	0.026	0.015	0.014	0.067
1.65	1.52	0.95	1.23	0.59	1.61	4.15
0.10	0.12	0.12	0.70	0.48	0.16	0.94
4.21	3.95	4.94	3.30	4.93	3.88	2.44
3.59	3.73	3.21	3.17	2.84	3.35	4.34
0.037	0.032	0.027	0.027	0.017	0.026	0.167
9	9	9	9	10	10	5
4	1	0	0	1	2	7
17	8	5	12	2	5	14
6	7	9	3	0	8	47
912	942	810	740	815	995	668
121	131	146	104	137	109	73
133	113	80	137	58	143	262
131	117	101	120	91	103	212
24	28	21	13	22	10	20
9.5	10.0	9.6	5.8	6.3	4.3	9.1
16	14	9	11	12	12	21
57	21	33	15	43	26	40
39	14	12	18	25	13	53
8	9	10	4	12	4	9
45	39	86	29	27	38	9
51	59	141	26	76	52	56
20	16	22	23	27	17	6

Rainier Fk Ridge granite	Miner's Ridge granite	Hwy 410 granodiorite	Rainier Fork Ridge granodiorite	Pear Butte Ridge granodiorite	Nelson Ridge granodiorite	Hwy 410 granodiorite
288	257	198	202	229	218	214
616964	624903	614685	618721	628691	630212	615230
5190933	5185291	5194006	5190665	5184545	5187134	5194037
76.36	76.42	67.82	68.03	68.03	68.52	68.64
13.68	12.96	16.48	15.79	15.92	16.04	15.18
0.162	0.123	0.660	0.518	0.484	0.462	0.545
0.41	1.10	3.99	4.34	4.02	2.92	4.17
0.009	0.016	0.105	0.046	0.057	0.054	0.083
1.37	1.00	2.08	2.55	3.66	3.94	2.96
0.01	0.04	2.06	1.21	0.95	1.28	1.39
4.57	4.89	2.45	2.93	2.33	2.19	2.64
3.42	3.42	4.20	4.41	4.40	4.50	4.26
0.007	0.018	0.170	0.189	0.136	0.109	0.134
11	10	10	5	7	18	8
3	2	4	3	5	16	7
2	4	15	7	20	10	13
0	6	32	30	43	57	32
893	806	441	819	684	607	608
148	135	71	101	83	43	62
106	79	130	203	257	586	158
133	93	261	241	202	118	232
22	23	46	24	19	10	40
10.7	10.3	12.9	16.6	11.1	7.8	14.3
17	15	15	20	16	16	17
17	6	5	107	62	27	12
0	14	59	33	42	53	53
5	9	14	8	7	12	8
21	24	15	34	19	21	32
44	60	61	74	39	48	79
12	23	6	8	11	4	6

APPENDIX B

XRF RESULTS

Hwy 410 granodiorite	Pear Butte Ridge granodiorite	American Ridge granodiorite	Pear Butte Ridge granodiorite	Rainier Fork Ridge granodiorite	Rainier Fork Ridge granodiorite	Nelson Ridge quartz diorite
199	228	196	232	206	207	155
614679	629055	621848	628455	617582	617988	630206
5194201	5182933	5190250	5182970	5192299	5192848	5185665
65.84	65.89	66.52	70.05	66.70	69.82	61.89
16.60	16.73	17.27	15.83	15.87	15.05	16.67
0.823	0.625	0.824	0.413	0.660	0.480	0.829
5.06	4.42	4.90	2.81	4.72	3.32	6.91
0.111	0.073	0.072	0.051	0.085	0.074	0.164
3.92	4.67	2.51	3.23	3.60	3.36	5.11
1.67	1.39	2.19	0.64	1.46	1.46	2.06
1.52	1.66	1.24	2.32	2.65	2.78	2.17
4.22	4.37	4.23	4.55	4.06	3.56	3.94
0.234	0.185	0.242	0.113	0.186	0.105	0.246
10	8	5	8	4	6	3
10	11	1	6	5	7	13
20	15	14	18	13	11	19
56	58	63	35	60	33	90
492	442	309	819	632	691	585
40	42	35	70	120	93	84
229	468	269	251	194	198	290
269	155	180	179	172	157	169
29	14	23	17	35	22	29
13.6	12.6	13.2	9.9	9.4	9.2	12.0
21	20	23	15	17	17	21
5	80	56	59	19	10	32
70	91	58	55	49	31	107
9	10	6	11	2	4	13
10	6	12	9	0	27	36
71	30	69	52	34	24	60
5	5	12	8	7	11	8

Nelson Ridge granodiorite	Miner's Ridge granodiorite	Nelson Ridge granodiorite	Nelson Ridge quartz diorite	Nelson Ridge quartz diorite	Copper Creek quartz diorite	Nelson Ridge quartz diorite
3	237	6	7	152	223	221
630063	626042	630381	630413	630636	629467	630533
5184794	5181158	5184587	5184556	5186738	5184726	5186787
69.32	69.39	69.64	63.18	64.04	64.68	65.22
15.77	15.32	16.11	17.38	17.53	17.31	16.89
0.520	0.444	0.430	0.720	0.561	0.580	0.544
3.60	3.64	3.42	6.04	5.54	5.38	5.02
0.040	0.071	0.040	0.110	0.100	0.092	0.081
3.59	3.23	3.15	5.13	4.65	4.21	4.30
0.99	0.76	0.69	1.29	0.86	0.77	0.68
1.62	3.01	1.62	1.87	1.83	2.30	2.33
4.39	4.02	4.78	4.03	4.69	4.46	4.74
0.140	0.111	0.120	0.250	0.194	0.209	0.187
6	7	8	5	3	4	10
6	7	3	6	2	5	13
12	11	12	17	17	13	9
55	32	38	79	20	25	9
506	866	493	576	445	623	610
79	86	86	77	82	87	90
246	228	232	294	296	266	274
205	176	181	193	184	141	206
18	21	16	27	27	34	30
9.4	10.0	9.2	9.8	10.6	13.6	14.5
16	18	20	21	19	20	18
29	16	337	18	27	70	57
37	50	37	63	67	89	56
3	12	5	6	6	16	3
33	41	43	41	26	32	29
55	54	28	47	60	42	64
8	11	13	6	7	9	8

APPENDIX B

XRF RESULTS

Nelson Ridge quartz diorite	Nelson Ridge quartz diorite	Hwy 410 quartz diorite	Nelson Ridge quartz diorite	Pear Butte Ridge andesite	Hwy 410 andesite	Swamp Lake Trail basaltic andesite	Swamp Lake basaltic andesite
4	156	200	222	227	276	264	265
630127	630582	614406	630733	628697	614073	620915	619370
5184698	5185506	5194732	5185476	5182951	5194570	5187424	5187273
62.69	62.73	62.96	63.04	62.42	62.27	56.85	56.65
18.60	17.32	16.90	17.52	16.53	15.50	17.64	17.56
0.670	0.809	1.001	0.728	1.081	1.229	1.106	1.095
4.68	6.25	6.29	5.09	6.80	7.33	6.97	6.93
0.060	0.077	0.145	0.111	0.088	0.175	0.119	0.123
4.34	4.64	4.96	5.08	4.40	4.95	7.24	7.19
1.62	1.41	2.01	1.27	2.27	1.66	4.82	5.27
1.97	1.65	1.06	2.22	2.04	1.58	1.12	1.13
5.16	4.87	4.40	4.71	4.22	4.92	3.96	3.86
0.210	0.238	0.273	0.229	0.159	0.386	0.183	0.189
7	1	4	6	7	2	53	64
8	4	2	2	12	2	107	129
14	17	19	16	20	26	24	23
70	51	72	54	203	58	138	153
668	372	349	610	257	388	267	273
111	104	31	80	181	49	26	26
275	281	247	283	202	228	466	466
186	246	213	160	120	202	129	126
21	27	39	29	40	46	19	19
11.1	10.2	15.1	12.4	12.6	15.7	8.7	9.0
22	21	21	20	21	19	15	17
15	89	28	22	10	12	24	27
48	62	80	59	59	71	62	70
4	11	6	11	7	7	3	7
25	29	20	41	24	24	6	21
65	35	59	45	64	65	38	17
12	6	1	8	10	5	3	6

Nelson Ridge quartz diorite	American Ridge rhyolite	Copper Creek dacite	American Ridge dacite of Toh
151	267	225	279
630412	619927	629624	621879
5187116	5188818	5185421	5192388
66.62	75.26	68.48	66.26
16.71	13.38	16.11	18.62
0.534	0.189	0.457	0.691
4.22	1.61	2.94	3.92
0.085	0.031	0.054	0.083
4.13	1.50	3.95	2.90
0.81	0.20	1.20	0.72
1.98	4.00	2.19	1.44
4.75	3.79	4.51	5.31
0.156	0.037	0.108	0.052
5	9	17	14
2	5	14	10
14	3	10	17
22	15	45	75
637	783	613	468
68	130	44	45
249	108	587	239
189	121	118	282
26	20	10	51
10.1	9.8	9.6	20.4
21	15	17	20
54	18	31	19
53	19	49	483
7	8	11	16
29	20	7	37
43	16	31	78
9	19	5	10

APPENDIX C

ICP-MS RESULTS

Description	aphanite	granite	granite	granite	granite	granite	granite	granite	granite	granodiorite	granodiorite	qtz diorite	xenolith
Chemical #	93162	93008	93010	93154	93182	93185	93188	93201	93206	93159	93214	93152	93187
Rb	168.41	100.92	66.23	105.06	124.79	97.37	125.19	136.15	115.44	67.38	56.39	76.38	31.42
Y	33.64	22.42	19.96	28.02	26.54	11.83	22.23	22.20	35.94	19.11	39.77	24.89	22.08
Nb	10.36	8.87	110.90	11.93	11.04	5.79	11.36	12.24	11.20	9.62	15.50	10.41	8.25
Cs	2.87	3.19	2.36	4.29	3.26	4.79	4.28	3.83	5.40	4.47	1.38	6.93	3.52
Ba	64.00	719.00	609.00	666.00	772.00	0.69	648.00	717.00	628.00	597.00	589.00	430.00	239.00
La	39.95	44.03	29.17	35.20	52.86	21.69	44.01	34.14	17.31	15.32	30.05	21.45	12.32
Ce	71.05	75.24	51.02	61.56	86.56	31.22	73.50	56.47	35.19	27.42	57.18	40.73	23.62
Pr	7.02	7.66	5.33	6.53	8.35	3.13	7.44	5.57	4.64	3.12	6.55	4.76	2.84
Nd	25.31	27.24	20.12	24.52	28.11	11.00	26.86	19.31	20.19	13.20	26.99	20.25	12.45
Pm	0.00	0.00	0.00	0.00	0.00	0.00	0.00	0.00	0.00	0.00	0.00	0.00	0.00
Sm	5.45	5.22	4.33	5.18	5.26	2.19	5.11	3.93	5.40	3.18	6.62	4.75	3.26
Eu	0.08	0.69	0.98	0.97	0.53	0.62	0.71	0.54	1.16	1.36	1.47	1.52	1.10
Gd	4.37	3.62	3.47	4.41	3.89	2.01	3.79	3.10	5.40	2.97	5.97	4.41	3.40
Tb	0.81	0.66	0.61	0.78	0.66	0.30	0.61	0.54	0.95	0.50	1.08	0.74	0.60
Dy	5.42	3.82	3.59	4.84	4.14	1.87	3.69	3.44	6.12	3.14	7.03	4.44	3.77
Ho	1.14	0.77	0.73	0.98	0.82	0.38	0.71	0.71	1.22	0.64	1.45	0.90	0.79
Er	3.64	2.21	1.96	2.74	2.49	1.04	2.10	2.11	3.57	1.91	4.10	2.41	2.24
Tm	0.56	0.32	0.29	0.41	0.36	0.15	0.30	0.32	0.49	0.27	0.58	0.34	0.31
Yb	3.81	2.28	1.78	2.59	2.34	0.94	1.99	2.18	3.01	1.73	3.79	2.21	1.92
Lu	0.61	0.36	0.28	0.42	0.39	0.15	0.33	0.35	0.47	0.30	0.59	0.35	0.31
Hf	3.68	2.92	3.32	3.57	2.86	2.40	2.82	2.52	3.42	4.36	4.82	3.67	2.58
Pb	14.16	7.86	6.99	10.90	11.09	5.85	7.79	9.14	3.97	8.82	10.28	6.61	10.71
Th	31.81	13.40	9.66	11.27	17.82	18.70	13.99	17.87	8.80	5.36	7.08	6.38	3.59
U	6.92	1.79	1.64	2.24	3.55	4.09	2.27	2.89	1.66	1.26	1.65	1.15	0.90